SIMULATING REMEDIATION OF TRICHLOROETHYLENE IN FRACTURED BEDROCK BY THERMAL CONDUCTIVE HEATING USING THE NUMERICAL MODEL TMVOC

by

Ashley McKenzie

A thesis submitted to the Department of Civil Engineering

in conformity with the requirements for

the degree of Master of Applied Science

Queen's University

Kingston, Ontario, Canada

(January, 2013)

Report Documentation Page

Form Approved
OMB No. 0704-0188

1. REPORT DATE	2. REPORT TYPE	3. DATES COVERED
JAN 2013		**00-00-2013 to 00-00-2013**

4. TITLE AND SUBTITLE	5a. CONTRACT NUMBER
Simulating Remediation of Trichloroethylene In Fractured Bedrock By Thermal Conductive Heating Using The Numerical Model TMVOC	5b. GRANT NUMBER
	5c. PROGRAM ELEMENT NUMBER
6. AUTHOR(S)	5d. PROJECT NUMBER
	5e. TASK NUMBER
	5f. WORK UNIT NUMBER
7. PERFORMING ORGANIZATION NAME(S) AND ADDRESS(ES) **Queen's University,Kingston, Ontario, Canada, , ,**	8. PERFORMING ORGANIZATION REPORT NUMBER
9. SPONSORING/MONITORING AGENCY NAME(S) AND ADDRESS(ES)	10. SPONSOR/MONITOR'S ACRONYM(S)
	11. SPONSOR/MONITOR'S REPORT NUMBER(S)

12. DISTRIBUTION/AVAILABILITY STATEMENT
Approved for public release; distribution unlimited

13. SUPPLEMENTARY NOTES
1/20, Government or Federal Purpose Rights License

14. ABSTRACT

A thermal conductive heating (TCH) pilot test was conducted at the Naval Air Warfare Center (NAWC) in West Trenton, New Jersey in 2009 in collaboration with TerraTherm, Inc., the Naval Facilities Engineering Services Center and the United States Geological Survey. The NAWC site was historically used as a jet engine testing facility from the mid-1950s to the late 1990s. During this time, the subsurface was contaminated with trichloroethylene (TCE) which was a common solvent used at the facility. The pilot test consisted of 15 heater/extraction wells installed to a depth of 16.8 m in weathered mudstone and operated for 102 days. Rock core samples were taken pre- and post-remediation to measure the initial TCE concentrations and evaluate the effect the TCH pilot test had. The data collected during the pilot test was used to create a two-dimensional (2D) finite difference model using TMVOC. TMVOC is part of the TOUGH 2 family of codes and is a numerical model that is capable of simulating multiphase flow, heat transfer and transport of volatile organic compounds in three-dimensional heterogenous porous media or fractured rock.

15. SUBJECT TERMS

16. SECURITY CLASSIFICATION OF:			17. LIMITATION OF ABSTRACT	18. NUMBER OF PAGES	19a. NAME OF RESPONSIBLE PERSON
a. REPORT	b. ABSTRACT	c. THIS PAGE			
unclassified	**unclassified**	**unclassified**	**Same as Report (SAR)**	**113**	

Abstract

A thermal conductive heating (TCH) pilot test was conducted at the Naval Air Warfare Center (NAWC) in West Trenton, New Jersey in 2009 in collaboration with TerraTherm, Inc., the Naval Facilities Engineering Services Center and the United States Geological Survey. The NAWC site was historically used as a jet engine testing facility from the mid-1950s to the late 1990s. During this time, the subsurface was contaminated with trichloroethylene (TCE) which was a common solvent used at the facility. The pilot test consisted of 15 heater/extraction wells installed to a depth of 16.8 m in weathered mudstone and operated for 102 days. Rock core samples were taken pre- and post-remediation to measure the initial TCE concentrations and evaluate the effect the TCH pilot test had. The data collected during the pilot test was used to create a two-dimensional (2D) finite difference model using TMVOC. TMVOC is part of the TOUGH 2 family of codes and is a numerical model that is capable of simulating multiphase flow, heat transfer and transport of volatile organic compounds in three-dimensional heterogenous porous media or fractured rock.

The 2D model was used as a screening model to investigate TCE removal from the rock matrix when heating for 100 days with a similar heating pattern to what was employed at the NAWC site. The numerical domain incorporated three primary fractures with competent bedrock in between. As the test pilot was conducted in the weathered bedrock zone, a sensitivity analysis was first completed on the matrix permeability to help to match the TCE removal from the pilot test. The pilot test had a 63.5% removal of TCE from the study area compared to 67% from the baseline model. A limited sensitivity analysis was completed which investigated how the matrix porosity and rate of energy application would have on the success of TCE removal from the rock matrix. It revealed that the TCE removal increases with increased matrix porosity and increased rate of energy application.

Acknowledgements

This research project was supported by the U.S. Department of Defence (DoD) Environmental Security Technology Certification Program (Project ER-0715) and Queen's University. Thank you to TerraTherm Inc., the United States Geological Survey (USGS), and the US Navy for their collaboration on this project.

Completing a Master's Thesis has been one of the most rewarding and challenging experiences of my life. I always had an interest in groundwater and contamination during my undergraduate studies, but having the opportunity to continue my education with graduate studies allowed me to explore these interests further. I would like to thank my thesis supervisor, Dr. Bernard Kueper for mentoring, inspiring and supporting me through this process. His willingness to answer all of my questions, have weekly meetings even if to just listen to my modeling frustrations and allow me to work and learn at my own pace has been greatly appreciated through this process.

Thank you to Ronald Falta at Clemson University who worked with me through model convergence errors and provided valuable insight into various aspects of the TMVOC model program.

I would like to thank my friends and family for supporting me through my ups and downs. To my parents for allowing me to escape University life when necessary and teaching me to never give up. Thank you to my husband, Brendan who always knows the right thing to say and for helping me brainstorm ideas whenever I became stuck on something. During my time at Ellis Hall I was fortunate to work in a positive office environment with some of the best people I know. Thank you to one of my greatest friends Titia Praamsma who not only let me invite myself to Africa, but

also stood by my side throughout my entire graduate career and knew when to make me laugh or go for a coffee break.

Table of Contents

List of Figures

List of Tables

Nomenclature

Latin Letters

A	area	[m^2]
b	Klinkenberg parameter	[Pa^{-1}]
C	solute concentration	[kg/m^3]
C_{dry}	de-saturated thermal conductivity	[W/m°C]
C_i	effective solubility	[mg/L]
c_p	specific heat capacity	[J/kg°C]
C_r	addition factor	
C_T	soil concentration	[mg/kg]
C_{wet}	saturated thermal conductivity	[W/m°C]
D	diffusion coefficient	[m^2/s]
e	fracture hydraulic aperture	[m]
F	mass or heat flux	[kg/m^2s] or [W/m^2]
f_{oc}	fraction of organic carbon	[-]
g	gravitational acceleration	[m/s^2]
h	convective heat transfer coefficient	[W/m^2K]
h_{fg}	latent heat of vapourization	[kJ/kg]
k	permeability	[m^2]
k_b	bulk permeability	[m^2]
k_{fz}	permeability of the fracture zone cells	[m^2]
k_f	calculated fracture permeability	[m^2]
k_∞	permeability at an infinite pressure	[m^2]
k_m	matrix permeability	[m^2]
k_o	intrinsic permeability	[m^2]

k_{oc}	organic carbon partition coefficient	[mg/L]
K	hydraulic conductivity	[m/s]
K_d	distribution coefficient	[ml/g]
K_d	soil-water partition coefficient	[mg/L]
l	interval length	[m]
m	mass of liquid boiled per unit time	[M/T]
M	mass accumulation	[kg/m^3]
n	normal vector	
P	pressure	[Pa]
P_{vap}	vapor pressure	[Pa]
q	rate of heat transfer	[W/m°C]
q_c	convective heat transfer rate	[W/m°C]
Q	heat flux	[W/m^2]
∇T	temperature gradient	[$^oC/m$]
S	saturation	[-]
T	temperature	[°C]
T_c	critical temperature	[°C]
T_∞	temperature of the fluid	[°C]
TR	transmissivity	[m^2/s]
T_w	temperature of the wall	[°C]
u	specific internal energy	[J/kg]
V	volume	[m^3]
x	mole fraction	[-]
z_{fz}	thickness of fracture zone cell	[m]

Greek Letters

α	thermal diffusivity	[m^2/s]
β	fluid phase	
γ	water, NCG, VOCs or heat component	
Δz_m	packer spacing	[m]
Δz_{fz}	fracture cell thickness in model	[m]
ε	compressibility	[Pa^{-1}]
ε_p	pore compressibility	[Pa^{-1}]
ε_b	bulk compressibility	[Pa^{-1}]
ε_T	expansivity	[1/°C]
θ	contact angle	[degrees]
κ	thermal conductivity	[W/m°C]
μ	viscosity	[g/s·cm]
ρ	density	[kg/m^3]
σ	interfacial tension	[N/m]
τ_g	gas phase tortuosity	[-]
$Ø_R$	reference porosity	[-]
Ø	porosity	[-]
$Ø_f$	fracture porosity	[-]
$Ø_m$	matrix porosity	[-]

Subscripts

a	air
g	gas phase
n	NAPL phase
p	constant pressure
R	rock
s	solid phase
v	constant volume
w	water phase

Chapter 1

Introduction

Groundwater and soil contamination by dense, non-aqueous phase liquids (DNAPLs) has been a continuing concern in North America since the early 1980s. Historical disposal methods, regulations and governance have resulted in tens of thousands of sites impacted by polychlorinated biphenyls (PCBs), creosote, coal tar, and various chlorinated solvents. The focus of this research is on the remediation of the chlorinated solvent trichloroethylene (TCE) in fractured bedrock. A numerical model capable of simulating three-phase non-isothermal flow of water, gas and multi-component mixtures of volatile organic compounds (VOCs) in multidimensional heterogeneous porous media was used to model a Thermal Conductive Heating (TCH) field pilot test that was conducted at a contaminated fractured bedrock site. The pilot test took place at the Naval Air Warfare Centre (NAWC) in West Trenton, NJ which was previously used as a jet engine testing facility, and decommissioned in 1998. The results from the model have been compared to the field test results to ascertain what properties of the bedrock and what features of the technology are most influential with respect to mass and concentration reduction.

Organic liquids immiscible with water are referred to as non-aqueous phase liquids (NAPLs). If the NAPL is less dense than water, it is referred to as a light, non-aqueous phase liquid (LNAPL); if it is denser than water, it is referred to as a dense, non-aqueous phase liquid (DNAPL). There are several classes of DNAPLs which include chlorinated solvents, coal tar, creosote, and PCBs (Kueper et al., 2004). In addition to being denser than groundwater, chlorinated solvent DNAPLs often have a lower viscosity than water, resulting in potentially rapid migration rates below the water table, particularly in fractured rock (Kueper and McWorter, 1991). It is difficult to predict the migration pathways of DNAPL when the geology at a site is complex as it often is with

fractured rock (Domenico & Schwartz, 1990). Upon release to the subsurface, DNAPL will come to rest as both disconnected blobs and ganglia of organic liquid referred to as residual DNAPL, and in continuous distributions referred to as pooled DNAPL (Kueper et al, 1997). Both residual and pooled DNAPL slowly dissolve into flowing groundwater, giving rise to aqueous phase plumes.

Due to inadequate knowledge and technology in the 20th century, it was unknown that chlorinated solvents could result in long-term contamination of the subsurface. Poor disposal and storage procedures resulted in many releases to the subsurface that were not properly remediated (Kueper et al, 2004). There are many sites in the United States and Canada that are contaminated with chlorinated solvent DNAPLs and are in need of remediation.

TCE is a common industrial degreaser and dry cleaning fluid that has been widely used by a variety of industries since the 1940s (Kueper et al, 2004). TCE has been shown to be harmful to humans if repeated or high levels of exposure occur (U.S. Department of Health and Human Services, 1997). Exposure can lead to acute and chronic health effects (U.S. Department of Health and Human Services, 1997). Stringent drinking water standards have been put in place for allowable levels of TCE, due to potential short-term and long-term health effects. In the province of Ontario, for example, the maximum allowable concentration of TCE in potable water is 5 μg/L (MOE, 2006, Table 2).

TCE was used at the NAWC facility from the mid-1950s to the late 1990s where jet engine testing occurred (Lacombe, 2000). The activities at the site resulted in TCE and other chemicals being released into the subsurface. A pump-and-treat system has been in place at the NAWC site since mid-1990 (Lacombe, 2011). The site is underlain by fractured sedimentary bedrock, primarily mudstone. Mudstone is a sedimentary rock that is composed of lithified mud and shale

(Aplin et al., 1999). A fissile mudstone is known as a mud-shale, while a non-fissile mudstone is referred to as mudstone (Aplin et al., 1999). Mudstones are classified primarily on grain-size and are typically composed of 1/3 to 2/3 silt sized fractions.

There are several remediation methods that have been used to address DNAPLs in the subsurface. These include pump-and-treat, hydraulic displacement, surfactant and co-solvent flushing, enhanced in situ bioremediation (EISB), in-situ chemical oxidation (ISCO), steam-enhanced extraction (SEE), electrical resistance heating (ERH), and thermal conductive heating (TCH). The remedial success of many of these methods in bedrock relies on the ability to flush fluids through the fracture network (Pankow and Cherry, 1996).

SEE, ERH and TCH are remediation methods that use heat to increase the subsurface temperature, thereby enhancing DNAPL removal (Triplett Kingston et al, 2010). In the application of SEE, a network of injection and extraction wells are used whereby steam is injected into the subsurface and the vapors and liquids are recovered for treatment (Johnson et al, 2009). The process creates a steam zone in the treatment area (Nilsson et al, 2011). The technology relies on the ability to deliver steam to the contaminated areas and therefore may be difficult to apply in fractured rock. A general limiting factor of SEE is that the boiling point of water is the maximum temperature that can be obtained.

ERH is similar to SEE in that the maximum obtainable temperature in the subsurface is the boiling point of water. This technology uses a network of electrodes to conduct electrical current through the subsurface, along with a network of extraction wells to collect liquids and vapours (Johnson et al, 2009). This technology performs best when there is ample moisture in the subsurface to maintain electrical conductivity. The effectiveness of ERH can be adversely affected by groundwater flow. If the groundwater velocity is sufficiently high, heat will be

carried away from the treatment zone at a rate sufficient to inhibit boiling. ERH is generally not applicable to fractured rock because of the excessively high electrical resistivity of most rock types.

TCH utilizes a network of wells containing a heating coil to heat the subsurface through conduction to temperatures reaching 500 degrees Celsius (°C) (Heron et al, 2009). This process is highly effective for volatile organic compounds such as chlorinated solvents as the dominant removal mechanism is by vaporization of the chlorinated solvent and collection of the subsequent vapors by extraction wells. Similar to ERH, the success of thermal conductive heating is reduced with increased groundwater flow. TCH has been successfully implemented at several contaminated sites. For example, in Memphis, Tennessee a site had levels of chlorinated compounds at concentrations greater than 1000 mg/kg. The site was underlain by low-permeability loess which was in turn underlain by high-permeability alluvium composed of sands, sands and gravels, and fluvial deposits (Heron et al, 2009). A volume of 38,200 m^3 was treated using TCH for 177 days (Heron et al, 2009). The site was remediated to concentrations less than 0.01 mg/kg, representing a 99.99% reduction in concentration.

1.1 Research Objectives

Thermal conductive heating applications have been implemented on many occasions in porous media with successful results (Johnson et al., 2009), but there is relatively little experience in fractured rock. . To evaluate the performance of TCH in fractured rock, a field pilot test was carried out by TerraTherm, Inc. in 2009 in collaboration with the Naval Facilities Engineering Services Center, Queen's University and the United States Geological Survey at the former Naval Air Warfare Center (NAWC) in West Trenton, New Jersey. Queen's University (David Rodriguez and Ashley McKenzie) assisted in data collection by measuring the trichloroethylene

concentrations in the rock pre- and post-remediation using methods developed by Rodriguez and Kueper, 2012). Using data gathered from site characterization activities at the NAWC site and the TCH pilot test, a finite difference model was created using TMVOC to evaluate the reduction of TCE concentrations in the rock matrix upon application of TCH.

TMVOC is a numerical model that is capable of simulating the flow and transport of multi-component VOCs in all three phases (gas-water-NAPL), above and below the water table in three-dimensional heterogeneous porous media, or fractured bedrock. It is able to simulate non-condensable gases as well as advection, dispersion, sorption, phase partitioning and biodegradation (Pruess and Battistelli, 2002). TMVOC allows for irregular grids to be created by using the Integral Finite Difference Method for space discretization. The model can simulate heat transfer applications such as thermal conductive heating and steam-enhanced extraction remediation technologies.

A radial symmetric screening model of the pilot test completed at the NAWC site was created. The temperature and mass removal data collected during the test pilot were used as input parameters to create the baseline model conditions. A limited sensitivity analysis was completed on the 2D model to evaluate which parameters are most influential on TCE removal from the rock matrix. The varied parameters in the sensitivity analysis were matrix permeability, matrix porosity and energy rate. From the results of this study, recommendations for future TCH remediation in fractured bedrock aquifers have been determined as well as future modeling recommendations.

1.2 Organization

Organization of the remaining Chapters and Appendices are as follows:

- Chapter 2 is a literature review that provides background information pertaining to the work completed for this project.
- Chapter 3 has been written as a standalone manuscript form intended for publication in Ground Water Monitoring and Remediation. Ashley McKenzie is the primary author of this paper and Bernard Kueper and Ronald Falta are the co-authors.

Supporting information for the project as well as the manuscript is contained in the Appendices which include:

- Appendix A – *TMVOC Governing Equations* which provides a brief summary of the equations that are used by TMVOC;
- Appendix B – *Model Testing* which examined if the numerical model was calibrated correctly by recreating an existing TMVOC model from the Users Manual;
- Appendix C – *TMVOC Model Input Property Definitions* which further explain the input parameters required for the numerical model simulations;
- Appendix D – *Calculations* that were required for select model input parameters; and,
- Appendix E – *Fixed versus No-Flow Bottom Boundary Condition* which examines the two different bottom boundary conditions considered when calibrating the baseline simulation.

1.2 Literature Cited

Aplin , A.C., Fleet, A.J., and MacQuaker, J.H.S. 1999. *Muds and mudstones: physical and fluid-flow properties.* Physical and Fluid Flow Properties 158:1-8.

Domenico, P.A., & Schwartz, F.W. 1990. *Physical and chemical hydrogeology.* Whiley, NY.

Heron, G., Parker, K., Galligan, J., & Holmes, T.C. 2009. *Thermal Treatment of Eight CVOC Source Zones to Near Nondetect Concentrations.* Ground Water Monitoring & Remediation 29, 56-65.

Johnson, P., Dahlen, P., Triplett, J., Foote, E., and Williams, S. 2009. *State-of-the-Practice Overview: Critical Evaluation of State-of-the-Art In Situ Thermal Treatment Technologies for DNAPL Source Zone Treatment*. ESTCP Project ER-0314.

Kueper, B.H., & McWhorter, D.B. 1991. *The behavior of dense, nonaqueous phase liquids in fracture clay and rock.* Ground Water 29, 716-728.

Kueper, B. H., Pitts, M., Wyatt, K., Simpkin, T., & Sale, T. 1997. *Technology Practices Manual for Surfactants and Cosolvents.* Online Document: Environmental Protection Agency. <http://www.clu-in.org> (April 11, 2010).

Kueper, B.H., Wealthall, G.P., Smith, J.N.W., Leharne, S.A., & Lerner, D.N. 2004. *An illustrated handbook of DNAPL transport and fate in the subsurface.* Environment Agency R&D Publication, Bristol.

Lacombe, P.J. 2011. *Mass of Chlorinated Volatile Organic Compounds Removed by Pump-and-Treat, Naval Air Warfare Center, West Trenton, New Jersey, 1996-2010.* U.S. Geological Survey Scientific Investigations Report 2011-5003.

Lacombe, P.J. 2000. *Hydraulic Framework, Water Levels, and Trichloroethylene Contamination, Naval Air Warfare Center, West Trenton, New Jersey, 1993-97.* U.S. Geological Survey Water Resources Investigations Report 98-4167.

Ministry of Environment 2006. *Technical Support Document for Ontario Drinking Water Standards, Objectives and Guidelines.* PIBS#4449e01.

Nilsson, B., Tzovolou, D., Jaczalik, M., Kasela, T., Slack, W., Klint, K.E., Haeseler, F., & Tsakiroglou, C.D. 2011. *Combining steam injection with hydraulic fracturing for the in situ remediation of the unsaturated zone of a fractured soil polluted by jet fuel.* Journal of Environmental Management 92: 695-707.

Pankow, J.F., & Cherry, J.A. 1996. *Dense Chlorinated Solvents and other DNAPLs in Groundwater.* Waterloo Press, Portland, Oregon.

Pruess, K., & Battistelli, A. 2002. *TMVOC, A Numerical Simulator for Three-Phase Non-isothermal Flows of Multicomponent Hydrocarbon Mixtures in Saturated-Unsaturated Heterogeneous Media.* Lawrence Berkeley National Laboratory, Berkeley, CA.

Rodriguez, D.J., and Kueper, B.H. 2012. *Assessment of Thermal Conductive Heating for the Remediation of DNAPL Contaminated Fractured Bedrock.* (In Progress).

Triplett Kingston, J.L., Dahlen, P.R., & Johnson, P.C. 2010. *State-of-Practice Review of In Situ Thermal Technologies.* Ground Water Monitoring & Remediation 30: 64-74.

U.S. Department of Health and Human Services. 1997. *Toxicological Profile for Trichloroethylene.* Public Health Service, Agency for Toxic Substances and Disease Registry.

Chapter 2

Literature Review

Groundwater and soil contamination is a growing issue in North America. Previous disposal methods, regulations and governance have led to many types of contamination in the subsurface. The focus of this research is on chlorinated solvents, which have been used as industrial degreasers since the early 1900s. Remediation of these solvents can be challenging and is very site specific. Thermal conductive heating (TCH) is a technology that has successfully removed chlorinated solvents from porous media sites. It is a method by which a grid of wells containing a heating element heats the subsurface to above the boiling temperature of the chemical, with an extraction system at the surface to collect the vapors for further treatment. It is important to understand the characteristics of chlorinated solvents, thermal and fractured rock properties, as well as TCH before implementing this technology.

2.1 Chlorinated Solvents

Chlorinated solvents were introduced to North America in the 20th century when they were used as degreasers in manufacturing plants, and for many products such as fire extinguishers and refrigeration uses (Jackson & Dwarakanath, 1999). Chlorinated solvents are commonly referred to as dense non aqueous phase liquids (DNAPLs) that are composed of chlorinated hydrocarbons and can be single or multi-component compounds (Kueper et al, 2004). The most common chlorinated solvents are trichloroethylene (TCE), perchloroethylene (PCE) and carbon tetrachloride (CT), which were used since the 1960s by industry for a variety of purposes including metal degreasing and dry cleaning. Due to inadequate knowledge and technology in the 20th century, it was unknown that chlorinated solvents could contaminate the subsurface,

therefore disposal and storage procedures were poor, and many accidental spills occurred which were not properly cleaned up (Kueper et al, 2004).

Chlorinated solvents are heavier than water, which has a density of 998 kg/m^3 and a viscosity of 0.01005 g/cm·s at 20 degrees Celsius, as compared to common chlorinated solvent DNAPLs that have densities ranging from 1100 kg/m^3 to 1600 kg/m^3, and viscosities ranging from 0.0057 g/cm▪s to 0.01 g/cm▪s respectively (Fetter, 2001; Kueper et al, 2004). With a higher density than water, chlorinated solvents are able to migrate below the watertable, with potentially rapid rates of migration in the subsurface (Kueper et al, 2004).

There are many sites in the United States and Canada that are contaminated with DNAPLs, and are in need of remediation. It is difficult to predict the migration pathways of a DNAPL when the geology at the site is complex (Domenico & Schwartz, 1990). Figure 2-1 is an example of how DNAPL migration may occur in the subsurface (Kueper and McWhorter, 1991).

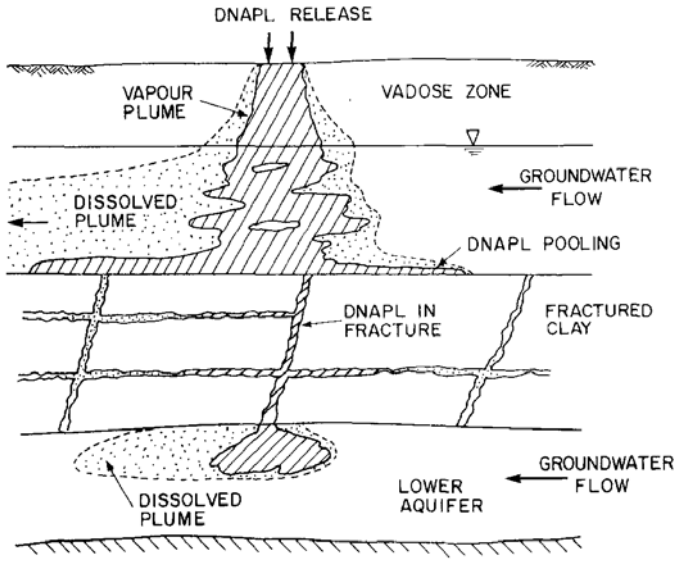

Figure 2-1 - Migration pathways due to DNAPL release into the subsurface (Kueper, & McWhorter, 1991).

Residual and pooled DNAPL will form as the DNAPL migrates through the subsurface (Kueper et al., 1997). Residual DNAPL is formed when the DNAPL migrates into pore spaces or fractures and becomes trapped by capillary forces as isolated blobs and ganglia of liquid. Residual DNAPL can occur in the saturated or unsaturated zone, and the amount of residual created varies according to many factors such as interfacial tension, the viscosity and density of the DNAPL, and the permeability of the medium (Kueper et al., 1997). Pooled DNAPL represents a continuous distribution of liquid through the pore spaces, and is found above capillary barriers typically associated with variations in permeability (Kueper et al., 1997).

Potable groundwater for generic site conditions have maximum acceptable concentrations of 0.5 μg/L for TCE and PCE, and 0.2 μg/L for CT as set by the Ministry of Environment (MOE, 2011, Table 1). Repeated exposure to these chemicals above the acceptable concentrations can lead to acute and chronic health effects which may even lead to death (Ajo-Franklin et al., 2006).

The focus of this study is on thermal remediation of TCE. The production of TCE began in 1923 for use in adhesives and for metal cleaning and degreasing (Pankow & Cherry, 1996). TCE is a non-flammable, colorless liquid with a sweet odor and burning taste (Irwin, 1997). In the 1970s production of TCE declined when several health concerns arose (Pankow & Cherry, 1996). TCE can break down into other dangerous substances such as dichloroethylene, chloromethane, and vinyl chloride, which are also dangerous if exposure occurs, and causes further soil contamination (Irwin, 1997). Table 2.1 displays the properties of TCE compared to water. When remediating TCE, these chemical properties are important to consider as they may be affected by temperature and pressure changes.

Table 2-1 - Physical and chemical properties of trichloroethylene in comparison to water.

Parameter	TCE	Water
Chemical Formula	C_2HCl_3	H_2O
Liquid density at 20°C	1460 kg/m^3 [a]	998 kg/m^3 [a, d]
Viscosity	0.0057 g/cm·s [b, c]	0.010050 g/cm·s [d]
Aqueous solubility	1100 mg/L [c]	Not defined
Surface tension with air	29.5 dynes/cm [a]	72.0 dynes/cm [a]
Maximum contaminant level	0.005 mg/L [a]	Not defined

[a] Ajo-Franklin, Geller, & Harris (2006).
[b] Jackson, & Dwarakanath (1999).
[c] Kueper et al (2004).
[d] Fetter (2001).

2.2 Fluid Properties

2.2.1 Viscosity

Viscosity is the measure of the resistance of a fluid to flow, which is caused by internal friction within a fluid (Knox et al., 1993, Mercer and Cohen, 1990). Chlorinated solvents are less viscous than water with a viscosity ranging from 0.57 to 1.0 cP compared to that of water at 1.0 cP (Kueper et al., 2004). A lower viscosity results in the chemical penetrating the subsurface more rapidly with easier migration (Mercer and Cohen, 1990; Pankow and Cherry, 1996). The viscosity of a fluid is inversely proportional to temperature. As the temperature of DNAPL increases, the viscosity decreases which results in a less viscous and more mobile fluid (O'Carroll & Sleep, 2007).

2.2.2 Interfacial Tension and Wettability

Interfacial tension and wettability are two properties of chlorinated solvents that are closely related. Interfacial tension is the force formed at the interface between two immiscible liquids, which prevents complete mixture of the fluids (Mercer and Cohen, 1990). Typical values for

interfacial tension for DNAPLs and water existing in the subsurface are between 5 and 35 mN/m (Kueper et al., 1997). These are less than textbook values because of the fact that small amounts of impurities typically lead to a reduction in interfacial tension (Dou et al., 2008). The interfacial tension between air and water is 72 mN/m, which is significantly greater than that between DNAPLs and water. The interfacial tension between two fluids will also be affected by the temperature. For example, as the temperature increases, the surface tension of air-water decreases (Vargaftik et al., 1983). The wettability is dependent on the interfacial tension of a chemical and is defined as the ability for a chemical to spread on a surface when present with another chemical (Dou et al, 2008; Mercer and Cohen, 1990). It is measured by the contact angle between the two fluids where the fluid-fluid interface meets the solid surface as displayed in Figure 2-2.

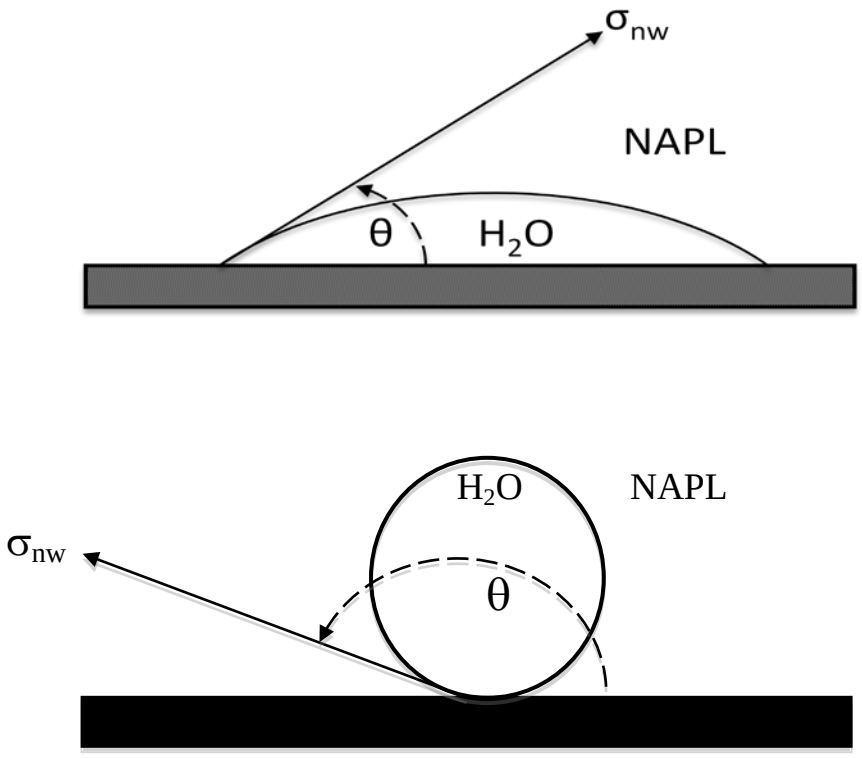

Figure 2-2 - (top) water-wet contact angle; (bottom) NAPL-wet contact angle (modified from Mercer & Cohen, 1990).

The two fluids are classified as either wetting or non-wetting depending on the contact angle. Young's equation represents the relationship between the contact angle and interfacial tension as follows (Mercer and Cohen, 1990):

$$cos\emptyset = \frac{(\sigma_{ns} - \sigma_{ws})}{\sigma_{nw}} \tag{2.1}$$

where ϕ is the contact angle, σ is the interfacial tension, *n* represents the NAPL phase, *s* represents the solid and *w* represents the water phase. When the contact angle is less than 70 degrees, the fluid through which that angle is measured is considered to be the wetting fluid, and the other is considered to be the non-wetting fluid. When the contact angle is close to 90 degrees, the system is considered to be neutral-wet (Mercer and Cohen, 1990; Donaldson and Alam, 2008).

2.2.3 Phase Change

When a liquid is subjected to a change in temperature or pressure, it can cause the liquid to change phases into a vapor. Temperature and pressure are very important parameters when examining DNAPLs as they are dependent for liquid-vapor mixtures. A distinction between the liquid-vapor phases can not always be made and this point is known as the critical point. It is the exact moment when the change occurs. Figure 2-3 shows three different phases: solid, liquid, and vapor for a pure substance when it is subjected to pressure and temperature in relation to the volume.

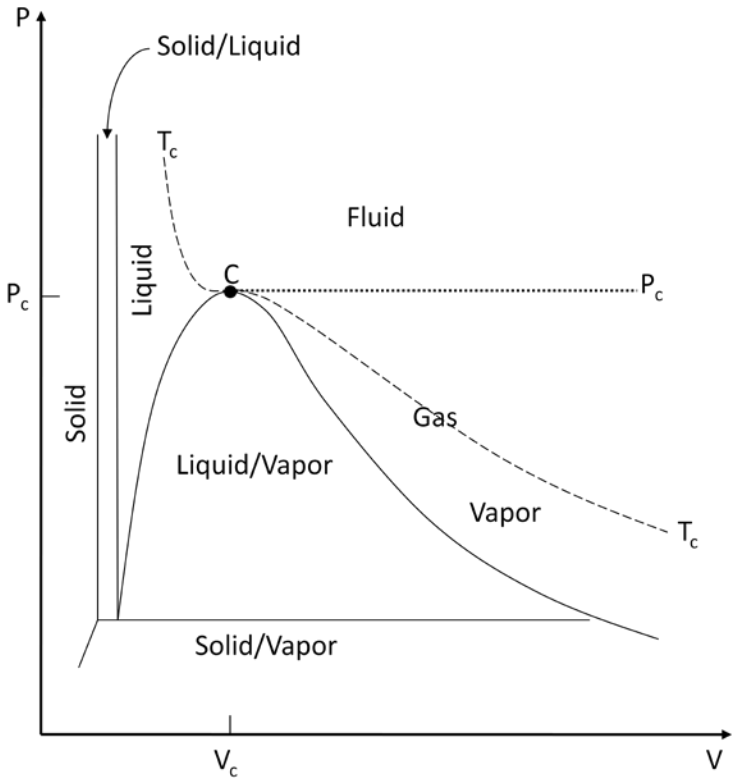

Figure 2-3 - Pressure-volume diagram for a pure substance (Smith et al, 1996).

The phase changes due to temperature and pressure can be describe by the equation of state and is described by Smith et al. (1996) as:

$$dV = \left(\frac{\partial V}{\partial T}\right)_P dT + \left(\frac{\partial V}{\partial P}\right)_T dP \tag{2.2}$$

where *V* is the volume, *T* is the temperature, and *P* is the pressure. The equation of state can be solved for pressure, temperature, or volume and it is a function of the two remaining variables where the "partial derivatives have definite physical meaning and are measureable quantities" (Smith et al., 1996).

Boiling and condensation is an important consideration in phase change. The heat that is absorbed or released in the liquid-vapor phase is described by Naterer (2003) as:

$$h_{fg} = \frac{q}{m} \tag{2.3}$$

where h_{fg} is the latent heat of vaporization, q is the rate of heat transfer during boiling, and m is the mass of liquid boiled per unit time when examining the vapor phase and it is defined as the rate of vapor condensation on a cooled surface if evaluating the condensation phenomenon (Naterer, 2003).

2.3 Heat Transfer

2.3.1 Conduction

Conduction is a form of heat transfer that is driven by the temperature gradient; when the heat (or energy) moves from a high energy region to a low energy region (Holman, 1997). It is defined by Fourier's Law of conduction as defined by Thomas (1980) as:

$$q = -\kappa A \nabla T \tag{2.4}$$

here q is the heat transfer rate in units of W/m·C, κ is the thermal conductivity of the material, A is the area of the object being examined and ∇T is the temperature gradient. The second law of Thermodynamics states that heat is transferred in the direction of decreasing temperature or "downstream" which means that a negative sign is present in the equation to make the heat transfer rate positive (Thomas, 1980).

Equation 2.4 can be applied to a three-dimensional system where the thermal conductivity, *K*, is held constant to become:

$$\frac{\partial^2 T}{\partial x^2} + \frac{\partial^2 T}{\partial y^2} + \frac{\partial^2 T}{\partial z^2} + \frac{q}{K} = \frac{1}{\alpha}\frac{\partial T}{\partial \tau} \tag{2.5}$$

where α is the thermal diffusivity of the material. An increase in the thermal diffusivity indicates that the temperature will diffuse through the material at a faster rate (Simons, 2007).

2.3.2 Convection

Convection is a physical process of heat transfer that occurs at the surface of a moving fluid and can only occur in gases or liquids (Thomas, 1980; Simons, 2007). The equation used to quantify convection is also known as Newton's law of cooling and is defined by Holman (1997) as:

$$q_c = hA(T_w - T_\infty) \tag{2.6}$$

where q is the convective heat transfer rate, h is the convection heat transfer coefficient, A is the surface area, T_w is the temperature of the wall and T_∞ is the temperature of the fluid. Convection is dependent on viscosity, thermal conductivity, specific heat and the density of the fluid (Holman, 1997). There are two types of convection: forced or natural. Forced convection is when the motion or flow is caused by mechanical or induced external forces, and natural convection is caused by buoyancy forces which result in a temperature induced density gradient within the fluids (Thomas, 1980; Simons, 2007). When examining thermal remediation, convection would be caused by the migration of steam produced by boiling groundwater.

2.3.3 Radiation

Objects emit and absorb electromagnetic radiation, which occurs due to the vibrational and rotational molecular, atomic and subatomic particle movements (Thomas, 1980; Simons, 2007). Thermal radiation is emitted by physical matter (Thomas, 1980). Radiation can only occur through transparent or partially transparent bodies when electromagnetic radiation is involved (Simons, 2007).

2.3.4 Thermal Diffusivity

Thermal diffusivity is a temperature dependent property that governs the transient heat transport equation [2.5]. It is directly related to the thermal conductivity of the material, κ, and inversely related to the specific heat at a constant pressure, c_p. It is expressed by Cermak and Rybach (1982) as:

$$\propto = \frac{\kappa}{c_p \rho} \tag{2.7}$$

where α is the thermal diffusivity and ρ is the density of the material. Studies by Durham et al. (1987) have shown that thermal diffusivity is dependent on temperature at different pressures. It was found that as the temperature increases, the thermal diffusivity decreases. The experiment performed by Durham et al. (1987) also found that the diffusivity increases when the pressure on the rock material increases, although the change is not as significant as what is seen when there is an increase in temperature.

2.4 Rock Properties

Fractured rock is a very intricate system with many fractures and complex matrices in which the DNAPL can penetrate deep into the system. There are several important properties that extend

beyond the specific description of the rock type such as porosity, compressibility, thermal conductivity, heat capacity and the effects of temperature and pressure on these properties.

2.4.1 Porosity

Porosity is defined as the volume of the voids or open pore spaces divided by the total volume of the media under consideration. There are two types of porosities: primary and secondary. The primary porosity is created when the rock is formed and the secondary porosity is created due to geological processes such as weathering, fracturing, etc. (Singhal and Gupta, 1999). The porosity value is controlled by many different factors such as the "shape and arrangement of constituent grains, degree of sorting, compaction and cementing, fracturing, and solution" (Singhal and Gupta, 1999). The total porosity of the rock is the sum of the matrix porosity and the fracture porosity and is shown in the equation below (Singhal and Gupta, 1999):

$$\emptyset = \emptyset_m + \emptyset_f \tag{2.8}$$

The porosity of the matrix (primary porosity), $\emptyset_m$, is the matrix void volume divided by the total volume where the matrix voids are formed due to intergranular void spaces (Singhal and Gupta, 1999). The fracture porosity (secondary porosity), $\emptyset_f$ is equal to the fracture void volume divided by the total bulk volume (Singhal and Gupta, 1999). The porosity can vary greatly for different types of rock and it depends on the rock location as well as historical exposure and geological events.

2.4.2 Compressibility

The total effective compressibility for fractured rock systems consists of three types of compressibility: rock matrix compressibility, rock bulk compressibility and pore compressibility.

All three must be taken into consideration when heat is being applied to the system, as the compressibility properties will be changed due to changes in pressure (Fatt, 1958). A change in the internal stress can occur when there is a decrease in the amount of fluid in the pore spaces of the rock. This stress change results in changes in the matrix, bulk, and pore compressibility in the rock (Jalalh, 2006). The bulk and pore compressibility are especially dependent on pressure because if the pressure is low then the compressibility will be greater than if the pressure was high (Geertsma, 1957). Compressibility is also a factor of the porosity as it can vary greatly between different rock types. When a rock is subject to confining pressure and internal pore pressures, compression of the rock occurs.

If there is a change in pressure it results in a fractional change of the solid rock material (i.e., the grains), which is known as the rock matrix compressibility (also known as the grain compressibility) (Amyx et al, 1960; Muggeridge et al, 2005; Geertsma, 1957). This compressibility is the least important compared to the rock bulk compressibility and the pore compressibility. When the porosity is greater than 0.15, the value of the rock bulk compressibility becomes much larger than the matrix compressibility. and thus it is considered negligible with respect to the bulk compressibility (Geertsma, 1957).

The rock bulk compressibility occurs when there is a “fractional change in volume of the bulk volume of the rock with a unit change in pressure” (Amyx et al, 1960, pg 58). The bulk volume of the rock is the volume if the pores are ignored (Zimmerman, 1991). This compressibility is important to consider if investigating under-saturated reservoirs because if a pressure is applied to the system then the rock will expand because it is directly proportional to pressure (Hall, 1953). A large expansion of the rock can alter the performance predictions of a reservoir (Hall, 1953).

The third compressibility to consider is the pore compressibility. When a change in pressure occurs, there is a change in the pore volume of the rock (Hall, 1953). Laboratory experiments performed by Jalalh (2006) showed that as the porosity of the rock increases, the pore volume compressibility exponentially decreases. If the porosity of the rock is very low, then this results in higher pore compressibility and makes the variable important for consideration when examining fractured rock systems (Geertsma, 1957).

Bulk compressibility and pore compressibility of bedrock are described by Zimmerman (1991) as:

$$\varepsilon_{ij} = \frac{-1}{V_i}\left[\frac{\partial V_i}{\partial P_j}\right]_{Pk} \tag{2.9}$$

where ε is the compressibility, i represents either the bulk volume or pore volume, and j is the stress on the rock, which is either confining pressure or the internal pore pressure. The bulk volume is defined as the volume of the pores and the rock minerals while the pore volume is the portion of the bulk volume that is not occupied by the rock minerals. V is the volume of the rock and $\partial V_i/\partial P_j$ is the change in volume due to the changing pressure with the secondary pressure, k, being held constant.

There are internal and external stresses present in rock bulk and pore compressibility. The internal stress is usually hydrostatic because it is usually due to a fluid. The pore pressures are varied and the external pressure is held constant (Geertsma, 1957). The external stress can vary in different directions as it is due to the rock stresses and is when the stress on the outer surface of the rock is changing and the internal (fluid) pressure is held constant (Geertsma, 1957).

2.4.3 Thermal Conductivity

Thermal conductivity is a property that is affected by the change in several other properties such as porosity, permeability, mineralogy and specific surface area and temperature (Midttoomme and Roaldset, 1998). It is defined by Fourier's Law, which states that the heat flux, *Q*, is equal to the thermal conductivity, κ multiplied by the temperature gradient, ∇T .

$$Q = -\kappa \nabla T \tag{2.10}$$

Porosity plays an important role when determining the thermal conductivity. Laboratory studies performed by Brigaud and Vasseur (1989), Thomas et al. (1973) and Midttoomme and Roaldset (1998) show that as the porosity of a material increases, the thermal conductivity decreases.

The decrease in thermal conductivity is greater when the porosity is smaller. As the porosity increases, the change in thermal conductivity decreases, displaying a non-linear trend (Brigaud and Vasseur, 1989). The thermal conductivity of a fluid or air is less than that of the grain material, thus as the porosity increases, there are more voids for the fluid or air to reside in which results in a decrease of thermal conductivity (Cermack and Rybach, 1982; Midttoomme and Roaldset, 1998).

Temperature and pressure also play an important role on the change in thermal conductivity. Changes in pressure cause the pores and microcracks in the rock to close resulting in more thermal contact resistance (when grains come into contact they create a path of heat flow resistance), which increases the thermal conductivity (Cermack and Rybach, 1982; Midttoomme and Roaldset, 1998). The increase of thermal conductivity occurs when lower pressures are applied to the rock because of rapid changes when the cracks initially close (Abdulagatov et al,

2006). Once higher pressures are applied, the change in thermal conductivity is insignificant (Abdulagatov et al., 2006).

The thermal conductivity is inversely proportional to the temperature of the rock (Cermack and Rybach, 1982). The increase in temperature causes a decrease in the thermal conductivity. The dependence on temperature is largely a factor of the skeletal properties of the rock material such as the mineral components (Abdulagatov et al, 2006).

2.4.4 Heat Capacity

The specific heat capacity, c_p, is the amount of heat that is required to increase the temperature of a material by 1 degree Celsius. The heat capacity varies by temperature and pressure. Equation 2.7 above shows the equation for the heat capacity as expressed by Cermak and Rybach (1982).

2.5 Thermal Conductive Heating

Thermal conductive heating (TCH), also known as in situ thermal desorption (ISTD), is an emerging technology in the groundwater remediation field. The remediation process uses a series of wells with heating elements inserted in each well. An electrical current is provided at ground surface to the heating elements. Figure 2-4 shows a fully installed and operable ISTD setup.

Figure 2-4 - Complete setup of the thermal conductive heating technology (TerraTherm, Inc.).

The heating element can reach temperatures of 800 degrees Celsius. Resistive heating takes place in the well and the process of conductive heating occurs away from the well (Baston and Kueper, 2009). This process is highly effective for chlorinated solvents as the dominant removal mechanism is by vaporization (Heron et al, 2009). When the chemical is heated, vapors (steam) are created, which are extracted by a vacuum system. Wells are typically placed 6 to 12 ft apart to ensure complete heating of the source zone when dealing with semi-volatile organic compounds and 12 to 20 ft for volatile organic compounds (Johnson et al, 2009).

TCH is not as dependent on the fracture spacing for the heat to be distributed as it is in steam injection. Another benefit of ISTD compared to that of electrical resistance heating is that the heating temperature can exceed 100 degrees Celsius, which is a major constraint of ERH (Kunkel et al, 2006). Also of note is the fact that ERH cannot be applied in many rock types because of the excessively high electrical resistivity of the rock matrix.

When TCH is applied, volatile organic compounds are destroyed by the following mechanisms as described by Baker et al. (2006): (i) evaporation, (ii) steam distillation, (iii) boiling, (iv) hydrolysis, (v) oxidation, and (vi) pyrolysis.

With any remediation technology, groundwater sources can pose a problem as an inflow of groundwater can reduce the heating in the system. To reduce the heat losses, the incoming groundwater can be boiled by either steam injection or placement of an extra row of heater wells outside of the treatment zone to preheat the water (Baston and Kueper, 2009). To reduce the amount of cooling that occurs, especially when high temperatures are desired, an insulation blanket will be placed over the surface of the treatment area in the form of a concrete slab (Baston and Kueper, 2009). This not only reduces heat loss, but also reduces the amount of infiltration of precipitation into the system.

Thermal conductive heating has been successfully implemented at contaminated sites. A study done by Triplet Kingston et. al (2010) found that from 1988 to 2007 there have been 26 pilot/field scale TCH applications with 17 of these being completed since 2000. The study concluded that there has been only one field scale application performed in weathered bedrock with the remaining applications conducted in porous media settings.

Examples of TCH applications include:

- Baker et al, (2006) discussed a former manufactured gas plant site in North Adams, Massachusetts in which residual coal tar was remediated with TCH inside of a brick walled gasholder of 5.5 m depth which was backfilled with a mixture of silt, sand gravel and cobbles and debris. The contaminates observed include naphthalene, benzo(a)pyrene, benzene and other Petroleum hydrocarbons (PHCs). The gasholder was heated for 3

months at low temperatures and then temperatures of 325°C were sustained for 9 months. There was a 96.43 to 99.98% reduction in concentration measured in the treatment zone.

- Heron et al. (2008) used TCH to remediate a site in southeastern U.S. which had a trichloroethylene source zone that extended 90 ft below the ground surface. The treatment zone geology consisted of 25 ft of fill underlain by 30 ft of severely weathered granitic gneiss, 20 ft of weathered bedrock and fractured bedrock at the bottom of the treatment zone. The treatment zone was heated at an average temperature of 100°C for 110 days. Starting soil and rock concentrations were measured to be as high as 81,000,000 µg/kg and was reduced to 17 µg/kg post treatment. The groundwater concentration in the treatment zone was reduced by 74.5 to 99.7%.

- Baker et al. (2007) discussed the remediation of a contaminated site in Southern California Edison, U.S. The treatment zone consisted primarily of silty soils which were contaminated with polycyclic aromatic hydrocarbons (PAHs), pentachlorophenol (PCP), and polychlorinated dibenzodioxins and furans (PCDD/Fs). The treatment zone was a maximum depth of 32 m and the soil concentrations for PAHs, PCP and PCDD/Fs were measured to be an average of 30,600, 2,940 and 18 µg/kg pre-treatment respectively. The subsurface was heated for 30 days at 300°C which resulted in reduced soil concentrations to 59, 1,250 and 0.11 µg/kg for PAHs, PCP and PCDD/Fs respectively which was below the remedial goal for the site.

2.6 Literature Cited

Abdulagatov, I.M., Emirov, S.N., Abdulagatova, Z.Z., Askerov, S.Y. 2006. Effect *of Pressure and Temperature on the Thermal Conductivity of Rocks.* J. Chem. Eng. Data 51, 22-33.

Ajo-Franklin, J.B., Geller, J.T., & Harris, J.M. 2006. *A survey of the geophysical properties of chlorinated DNAPLs.* Journal of Applied Geophysics 59, 177-189.

Amyx, J.W., Bass, D.M., & Whiting, R.L. 1960. *Petroleum Reservoir Engineering: Physical Properties.* McGraw-Hill Book Company, Inc. New York. REF # TN870 .A53 v.1

Baker, R.S., Brogan, D., & Lotti, M. 2006. *Demonstration of tailored levels of in situ heating for remediation of a former MGP site.* Land Contamination and Reclamation 14(2), 335-339.

Baker, R.S., Tarmasiewicz, D., Bierschenk, J.M., King, J., Landler, T., & Sheppard, D. 2007. *Completion of In-Situ Thermal Remediation of PAHs, PCP and Dioxins at a Former Wood Treatment Facility.* IT3'07 Conference (May 14-18, 2007), Phoenix, AZ.

Baston, D.P. & Kueper, B.H. 2009. *Thermal conductive heating in fractured bedrock: Screening calculations to assess the effect of groundwater influx.* Advances in Water Resources 32, 231-238.

Brigaud, F., & Vasseur, G. 1989. *Mineralogy, porosity and fluid control on thermal conductivity of sedimentary rocks.* Geophysical Journal 98, 525-542.

Čermák, V., and Rybach, L. 1982. *Thermal conductivity and specific heat of minerals and rocks.* In G. Angenheister (Ed.) Landolt-Börnstein: Numerical Data and Functional Relationships in Science and Tehcnology, Group V (Geophysics and Space Research), Volume 1a (Physical Properties of Rocks), (pp. 305{343). Springer, Berlin-Heidelberg.

Domenico, P.A., & Schwartz, F.W. 1990. *Physical and chemical hydrogeology.* Whiley, NY.

Donaldson, E.C., & Alam, W. 2008. *Wettability*. Gulf Publishing Company, Houston, Texas.

Dou, W., Omran, K., Grimberg, S.J., Denham, M., & Powers, S.E. 2008. *Characterization of DNAPL from the U.S. DOE Savannah River Site.* Journal of Contaminant Hydrology 97, 75-86.

Durham, W.B., Mirkovich, V.V., & Heard, H.C. 1987. *Thermal Diffusivity of Igneous Rocks at Elevated Pressure and Temperature.* Journal of Geophysical Research 92 (B11), 11615-11634.

Fatt, I. 1958. *Pore Volume Compressibilities of Sandstone Reservoir Rocks.* J. Petroleum Technology 10, 64-66.

Fetter, C.W. 2001. *Applied Hydrogeology: Fourth Edition.* Prentice Hall, New Jersey.

Jackson, R.E., & Dwarakanath, V. 1999. *Chlorinated degreasing solvents: physical-chemical properties affecting aquifer contamination and remediation.* Ground Water Monitoring & Remediation 19, 102-110.

Geertsma, J. 1957. *The Effect of Fluid Pressure Decline on Volumetric Changes of Porous Rock.* Trans AIME 210, 331-340.

Hall, H.N., 1953. *Compressibility of Reservoir Rocks.* Petroleum Transactions, AIME 198, 309-311.

Heron, G., Baker, R.S., Bierschenk, J.M., & LaChance, J.C. 2008. *Use of Thermal Conductive Heating for the Remediation of DNAPL in Fractured Bedrock.* Remediation of Chlorinated and Recalcitrant Compounds: Proceedings of the Sixth International Conference (May 19-22, 2008). Batelle Press, Columbus, OH.

Heron, G., Parker, K., Galligan, J., & Holmes, T.C. 2009. *Thermal Treatment of Eight CVOC Source Zones to Near Nondetect Concentrations.* Ground Water Monitoring & Remediation 29, 56-65.

Holman, J.P. 1997. *Heat Transfer: 8th Edition.* McGraw-Hill, Inc., United States.

Irwin, R.J. 1997. *Environmental Contaminants Encyclopedia: Trichloroethylene Entry*. Fort Collins, Colorado.

Jalalh, A.A. 2006. *Compressibility of porous rocks: Part II. New relationships.* Acta Geophysica 54(4), 399-412.

Johnson, P., Dahlen, P., Triplett, J., Foote, E., and Williams, S. 2009. *State-of-the-Practice Overview: Critical Evaluation of State-of-the-Art In Situ Thermal Treatment Technologies for DNAPL Source Zone Treatment.* ESTCP Project ER-0314.

Knox, R.C., Sabatini, D. A., & Canter, L.W. 1993. *Subsurface Transport and Fate Processes.* Lewis Publishers, Boca Raton, Florida.

Kueper, B.H., & McWhorter, D.B. 1991. *The behavior of dense, nonaqueous phase liquids in fracture clay and rock.* Ground Water 29, 716-728.

Kueper, B. H., Pitts, M., Wyatt, K., Simpkin, T., & Sale, T. 1997. *Technology Practices Manual for Surfactants and Cosolvents.* Online Document: Environmental Protection Agency. <http://www.clu-in.org> (April 11, 2010).

Kueper, B.H., Wealthall, G.P., Smith, J.N.W., Leharne, S.A., & Lerner, D.N. 2004. *An illustrated handbook of DNAPL transport and fate in the subsurface.* Environment Agency R&D Publication, Bristol.

Kunkel, A. M., Seibert, J. J., Elliott, L. J., Kelley, R., Katz, L. E., & Pope, G. A. 2006. *Remediation of elemental mercury using in situ thermal desorption ISTD.* Environmental Science & Technology 40, 2384-2389.

Mercer, J.W., & Cohen, R.M. 1990. *A Review of Immiscible Fluids in the Subsurface: Properties, Models, Characterization and Remediation.* Journal of Contaminant Hydrology 6, 107-163.

Midttømme, K., & Roaldset, E. 1998. *The effect of grain size on thermal conductivity of quartz sands and silts.* Petroleum Geoscience 4, 165-172.

Ministry of Environment 2011. *Soil, Ground Water and Sediment Standards for Use Under Part XV.1 of the Environmental Protection Act.* PIBS#7382e01.

Muggeridge, A., Abacioglu, Y., England, W., & Smalley, C. 2005. *The rate of pressure dissipation from abnormally pressured compartments.* AAPG Bulletin 89(1), 61-80.

Naterer, G.F. 2003. *Heat Transfer in Single and Multiphase Systems.* CRC Press LCC, Boca Raton, Florida.

O'Carroll, D. M., Sleep, B. E. 2007. *Hot water flushing for immiscible displacement of a viscous NAPL.* Journal of Contaminant Hydrology 91, 247-266.

Pankow, J.F., & Cherry, J.A. 1996. *Dense Chlorinated Solvents and other DNAPLs in Groundwater.* Waterloo Press, Portland, Oregon.

Schärli, U., & Rybach, L. 2001. *Determination of Specific Heat Capacity on Rock Fragments.* Geothermics 30, 95-110.

Singhal, B.B.S., & Gupta, R.P. 1999. *Applied Hydrogeology of Fractured Rocks.* Kluwer Academic Press, Netherlands.

Simons, S.J.R. 2007. *Concepts of Chemical Engineering 4 Chemists.* RSC Publishing, Cambridge, United Kingdom.

Smith, J.M., Van Ness, H.C., & Abbott, M.M. 1996. *Introduction to Chemical Engineering Thermodynamics: Fifth Edition.* McGraw-Hill Companies Inc., USA.

Thomas, L.C., 1980. *Fundamentals of Heat Transfer.* Prentice-Hall, Inc., Englewood Cliffs, New Jersey.

Thomas, J., Frost, R.R., & Harvey, R.D. 1973. *Thermal Conductivity of Carbonate Rocks.* Engineering Geology 7, 3-12.

Triplett Kingston, J.L., Dahlen, P.R., & Johnson, P.C. 2010. *State-of-Practice Review of In Situ Thermal Technologies.* Ground Water Monitoring & Remediation 30: 64-74.

Vargaftik, N. B., Volkov, B. N., & Voljak, L. D. 1983. *International Tables of the Surface Tension of Water.* J. Phys. Chem. Ref. Data 12, 817-820.

Zimmerman, R.W. 1991. *Compressibility of Sandstones*. Elsevier, New York, NY.

Chapter 3

Numerical Simulation of Trichloroethylene Remediation in Fractured Bedrock by Thermal Conductive Heating

Abstract

A thermal conductive heating (TCH) pilot test was conducted in 2009 at the Naval Air Warfare Center (NAWC) in West Trenton, New Jersey which was historically impacted by trichloroethylene (TCE). Rock samples were collected pre- and post-remediation inside of the test pilot area to assess TCE removal from the rock matrix. Using site-specific data collected during the pilot test, a two-dimensional finite difference model was created using TMVOC to investigate TCE removal from the rock matrix compared to the removal during the NAWC test pilot. In the baseline model simulation, TCE removal in the rock matrix simulation was 67% compared to 63.5% removal in the pilot test. The numerical model was used as a screening tool to examine what parameters affect the mass removal from the rock matrix during 100 days of heating. A limited sensitivity analysis examined the matrix permeability, matrix porosity and energy rate to the subsurface. The sensitivity analyses indicated that TCE mass removal increases with increased matrix porosity and increased rate of energy application.

Keywords: Thermal Conductive Heating, fractured bedrock, trichloroethylene, remediation, numerical model

3.1 Introduction

The remediation of dense, non-aqueous phase liquids (DNAPLs) such as creosote, coal tar and chlorinated solvents in bedrock is a challenging task given the discrete nature of flow through fractures and the potential for back diffusion of contaminants in many rock types. Technologies that rely upon fluid injection, such as steam injection, in-situ chemical oxidation, enhanced in-situ bioremediation, and co-solvent flushing are typically limited by sweep efficiency and a general inability to address contaminants sequestered in the low permeability porous rock matrix in a timely manner. Thermal conductive heating (TCH), which relies largely upon heat conduction rather than the delivery of injected fluids, has potential applicability in fractured rock because it can deliver heat to not only open fractures, but to the rock matrix as well.

TCH employs electrical heaters suspended inside a cased borehole to deliver energy to the surrounding formation and can achieve temperatures of up to approximately 500 °C (Heron et al., 2009). The heat migrates away from the heater borings by a combination of thermal conduction (driven by a temperature gradient) and convection (migration of steam produced by boiling ground water). Upon heating to the boiling point of water, steam is formed in-situ along with the transfer of contaminant mass to the vapor phase (Heron et al., 2009). Vapor and liquid recovery is typically achieved through vacuum extraction and conventional groundwater pumping, respectively. In addition to physical removal through vapor and liquid recovery, biological and chemical degradation mechanisms may occur during and after thermal remediation. These mechanisms may include thermal destruction by oxidation and pyrolysis near heating elements at temperatures of approximately 400^{o}C, microbial mineralization of NAPL components, and hydrolysis at elevated temperatures (Baker and Kuhlman, 2002). The required target temperature in the treatment zone as well as the treatment time varies depending on a number of factors including the properties of the target compounds and heat losses. Heat losses generally occur at

the surface, below and around the perimeter of the treatment zone and are influenced by groundwater flux (Baston and Kueper, 2009). To reduce heat loss, the heater borings are generally extended 1 to 2 m outside of the treatment zone (Johnson et al., 2009). The general physical layout of a TCH application, including depiction of a power supply, produced fluids treatment components, temperature monitoring points, and pressure monitoring points is illustrated in Figure 3-1.

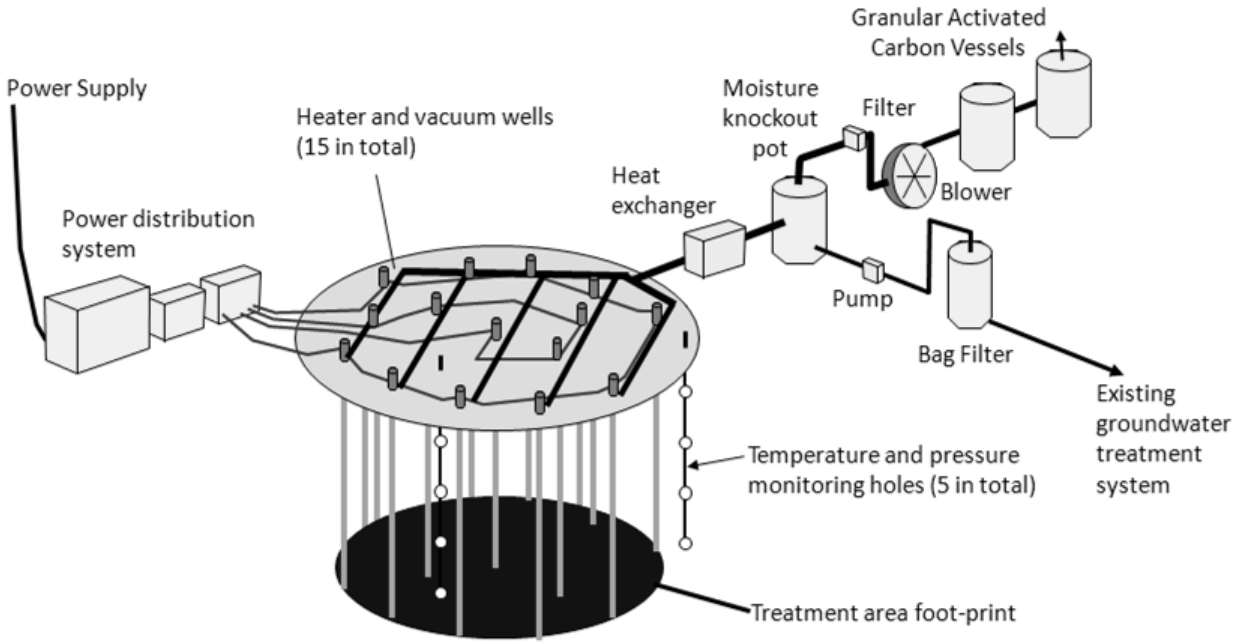

Figure 3-1 – Typical configuration for thermal conductive heating (Johnson et al., 2009, Appendix A: Heron and Baker).

TCH has been implemented on many occasions in porous media (Triplett Kingston et al., 2010), but there is relatively little experience in fractured rock. To evaluate the performance of TCH in fractured rock, a field pilot test was carried out by TerraTherm, Inc. in 2009 in collaboration with the Naval Facilities Engineering Services Center, Queen's University and the United States Geological Survey at the former Naval Air Warfare Center (NAWC) in West Trenton, New

Jersey. The NAWC facility operated from the mid-1950s to the late 1990s where it served as a U.S. Navy jet engine testing facility. Activities on the site resulted in the release of trichloroethylene (TCE) to bedrock.

Using data collected at the site during the pilot test and associated site characterization activities, a two-dimensional (2D) radial finite difference model was developed using TMVOC (Pruess and Battistelli, 2002). TMVOC is part of the TOUGH2 family of codes and is capable of simulating multiphase flow, heat transfer, and transport of volatile organic compounds (VOCs) in three-dimensional heterogeneous porous media or fractured rock (Pruess and Battistelli, 2002). The 2D model was developed as a screening tool to evaluate the reduction of TCE in the model to that of the pilot test when similar heating conditions were applied. A limited sensitivity analysis was conducted to focus on how the performance of TCE extraction was influenced by changes in matrix permeability, matrix porosity and energy input into the subsurface. The results from this study will generate recommendations for future TCH remediation applications in fractured bedrock aquifers.

3.2 TCH Pilot Test

A TCH pilot test was performed by TerraTherm Inc. at the NAWC facility between April 10 and July 24, 2009. A network of 15 heater/extraction wells (vapor and liquid extraction) was installed over an area of 45.6 m^2. The wells were installed to a depth of 16.8 m below ground surface (bgs) and screened their entire length to allow for maximum extraction of fluids. Further details pertaining to the pilot test are described in Rodriguez et al. (2012). Figure 3-2 illustrates the configuration of heater/extraction wells and temperature monitoring points associated with the field pilot test.

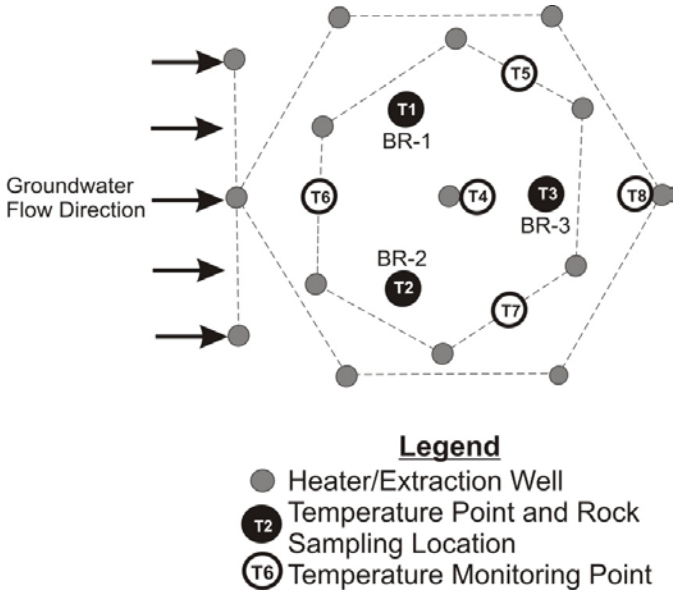

Figure 3-2 – Plan view configuration of heater/extraction wells and temperature monitoring points.

Three wells were installed on the upgradient side of the heating network to aid in reducing heat losses due to incoming groundwater flow. A total of eight temperature monitoring borings (T1 to T8) were completed with 10 temperature measurement points in each spaced at 1.52 m intervals beginning at 1.52 m below ground surface. A concrete cap was placed on top of the treatment zone to reduce heat losses at ground surface. The pilot test included combined heating and fluid extraction for 98 days, followed by fluid extraction alone for 4 days post-heating. Steady-state temperatures achieved in the treatment zone varied from approximately 60 °C to approximately 110 °C with an average of 98 °C (Figure 3-3). Temperatures in the bottom 4.6 m of the test interval did not reach 100 °C, likely because of the cooling influence of inflowing groundwater at those depths.

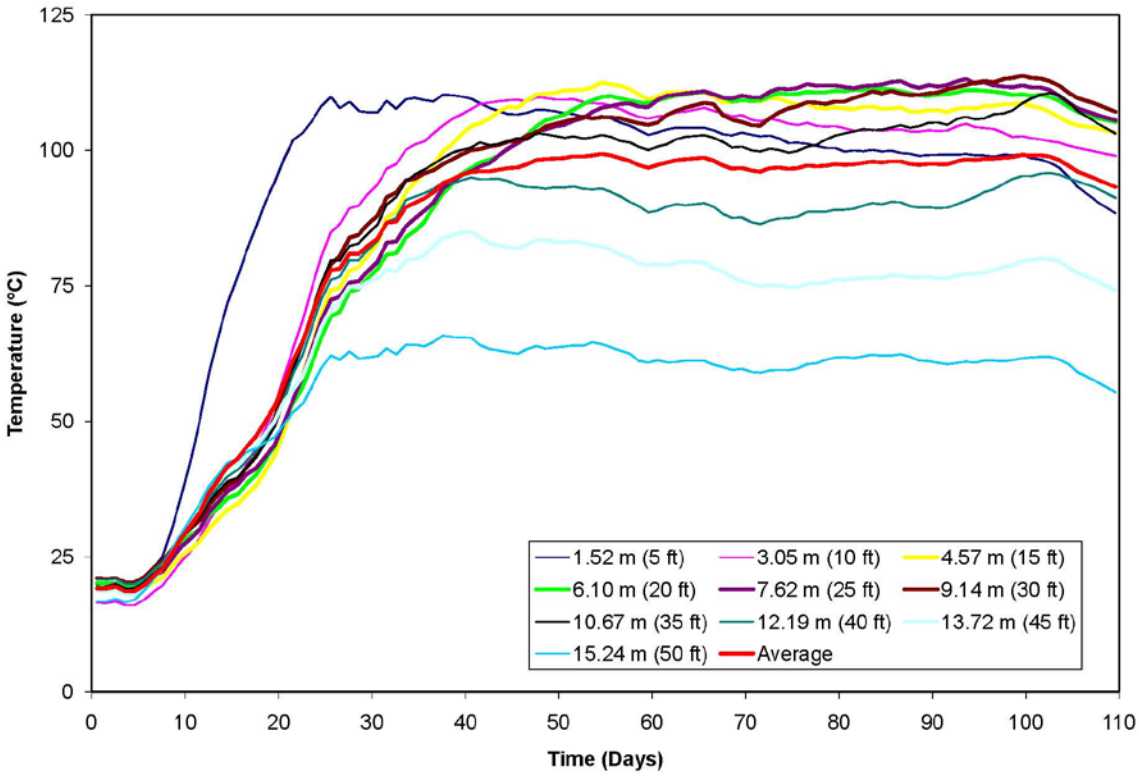

Figure 3-3 – Average temperature for eight temperature monitor borings (T1-T8) that had 1.52 m interval temperature points from 1.52 m to 15.24 m below ground surface during the NAWC pilot test (data provided by TerraTherm, Inc.).

To evaluate the removal of TCE from the rock matrix, three boreholes (BR-1, BR-2, and BR-3) were drilled in the centre of the treatment area in which samples were collected pre-treatment (Figure 3-2). Three additional boreholes were drilled and sampled post-treatment at locations adjacent to the pre-treatment boreholes. Rock samples were collected every 0.3 to 1.5 m with BR-1 containing the greatest density of sampling pre- and post-treatment. Rock samples were placed in a rock crushing device, preserved in methanol and shaken for 24 hours to allow the TCE to partition into the methanol (Rodriguez et al., 2012). The methanol solution was then extracted from each rock sample and analyzed for TCE concentration by an external laboratory. Figure 3-4 presents the rock matrix sampling results as a function of depth from the BR-1 pair of coring locations pre- and post-treatment. This location exhibited higher initial concentrations of TCE in

the rock matrix than BR-2 and BR-3. Considering results from all three paired locations, approximately 63.5% of the TCE was removed from the rock matrix as a result of TCH application.

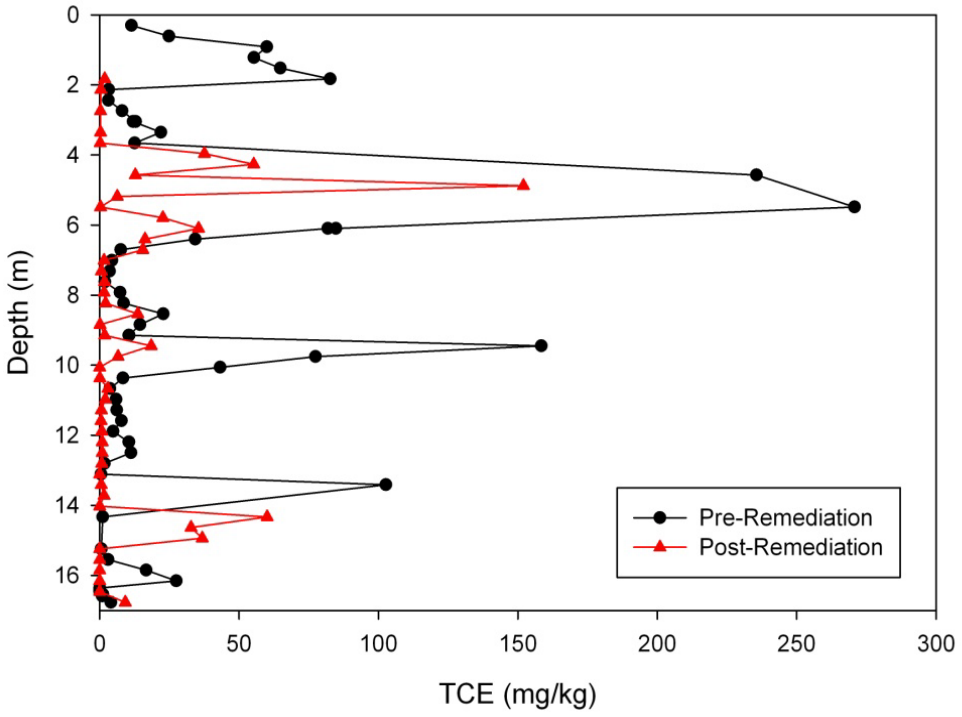

Figure 3-4 – TCE concentration in the rock matrix from location BR-1 pre- and post-treatment.

3.3 Model Development

3.3.1 Site Characterization Input

The NAWC Facility is underlain by mudstone bedrock that is part of the Lockatong Formation (Tiedeman et al., 2010; Lacombe and Burton, 2010). Figure 3-5 below displays a cross section of the geology at the NAWC Facility (Tiedeman et al., 2010) with the pilot test area highlighted.

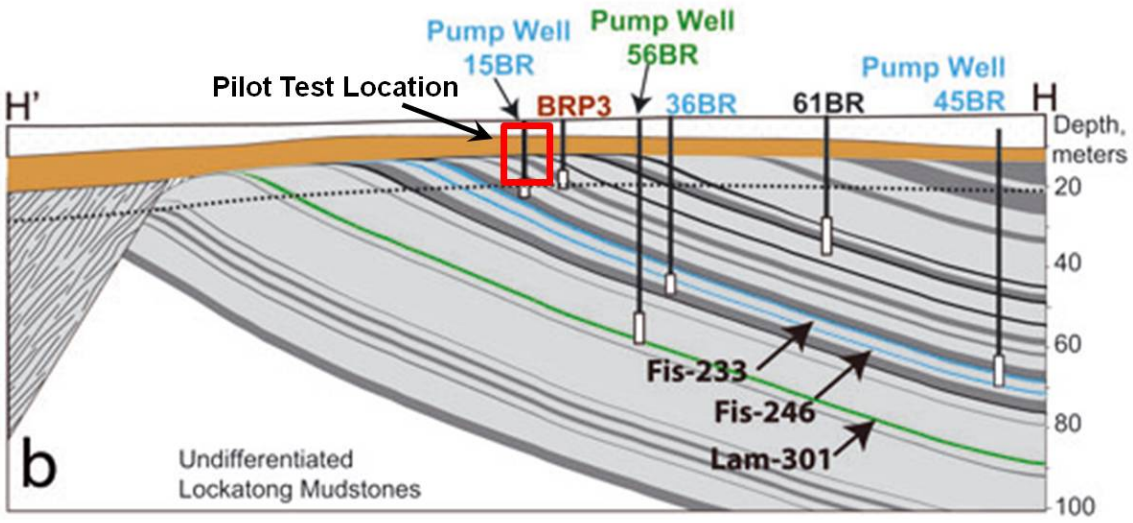

Figure 3-5 – Cross Section of the geology at the NAWC site with the pilot test location shown (Tiedeman et al., 2010).

The overburden material consists of a thin layer of fill and weathered saprolite which varies from 1 to 8 m in thickness across the NAWC site. In the area of the pilot test, the depth of this unit was to approximately 1.8 m below ground surface (bgs). The saprolite is composed primarily of silt and clay and has a bulk average permeability of 6.5×10^{-13} m^2 (Tiedman et al., 2010).

This layer is underlain by a highly fractured, weathered grey mudstone in which "the individual mudstone beds are difficult to distinguish" (Tiedeman et al., 2010). The weathered mudstone is underlain by dipping formations that alternate between beds of highly fractured mudstones which are highly conductive due to the inclined fractures; and more competent, less fractured beds (Tiedeman et al., 2010; Lewis-Brown et al., 2006). Laboratory testing completed on the mudstone rock in the area of the pilot test (from approximately 9.1 m bgs) was measured to have a bulk density of 2520 kg/m^3, a matrix porosity of 3.3%, a matrix permeability of 1×10^{-17} m^2 and a matrix fraction organic carbon of 0.0079 (average properties from Rodriguez et al., 2012). Hydraulic testing was completed by TerraTherm Inc. prior to the pilot test heating. This was done

by employing a straddle packer assembly and was conducted in the three holes in which the rock samples were taken. The bulk permeability of the pilot test area was measured to be $8.4x10^{-14}$ m^2. The bulk permeability is three orders of magnitude greater than the matrix permeability as the bulk permeability takes into consideration possible fracture networks in the weathered grey mudstone whereas the laboratory testing only considers a small rock core disk.

The water table across the NAWC Facility varies from 1 to 5 m below ground surface (Tiedeman et al., 2010) but in the area of the TCH pilot test, the water table was located 1.52 m bgs. The hydraulic gradient at the site in the pilot test area was approximately 0.008 (Tiedman et al., 2010).

3.3.2 Model Domain and Boundary Conditions

TMVOC was used to create a two-dimensional (2D) radial finite difference model to simulate TCE removal from the rock matrix using data collected from the pilot test. Figures 3-6 and 3-7 display the conceptual 2D model upon which the numerical model is based. The numerical simulations were designed to be radially symmetric to simulate the heater/extraction well that is located in the center of the well network (Figure 3-6).

The inside radius of the model domain is a symmetry boundary. The column of cells directly adjacent to this boundary (the first column of cells) has heating/extraction properties assigned. The outer radius of the domain was placed 1.5 m away and is subjected to no-flow conditions in order to model the symmetry boundary of a repeated pattern which represents the first ring of wells in the field test pilot.

The observation location is the outermost column of cells, which is located 1.25 m away (at the centroid of the cell column) from the center well. This location in the model represents the

location half way between the inner well and first ring of wells in the field pilot test which is approximately where the pre- and post-remediation rock samples were collected (BR-1 to BR-3).

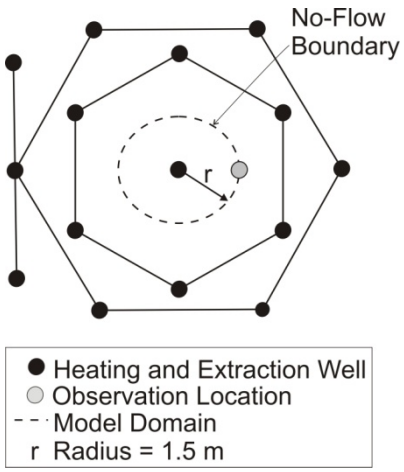

Figure 3-6 – Plan view of the conceptual model.

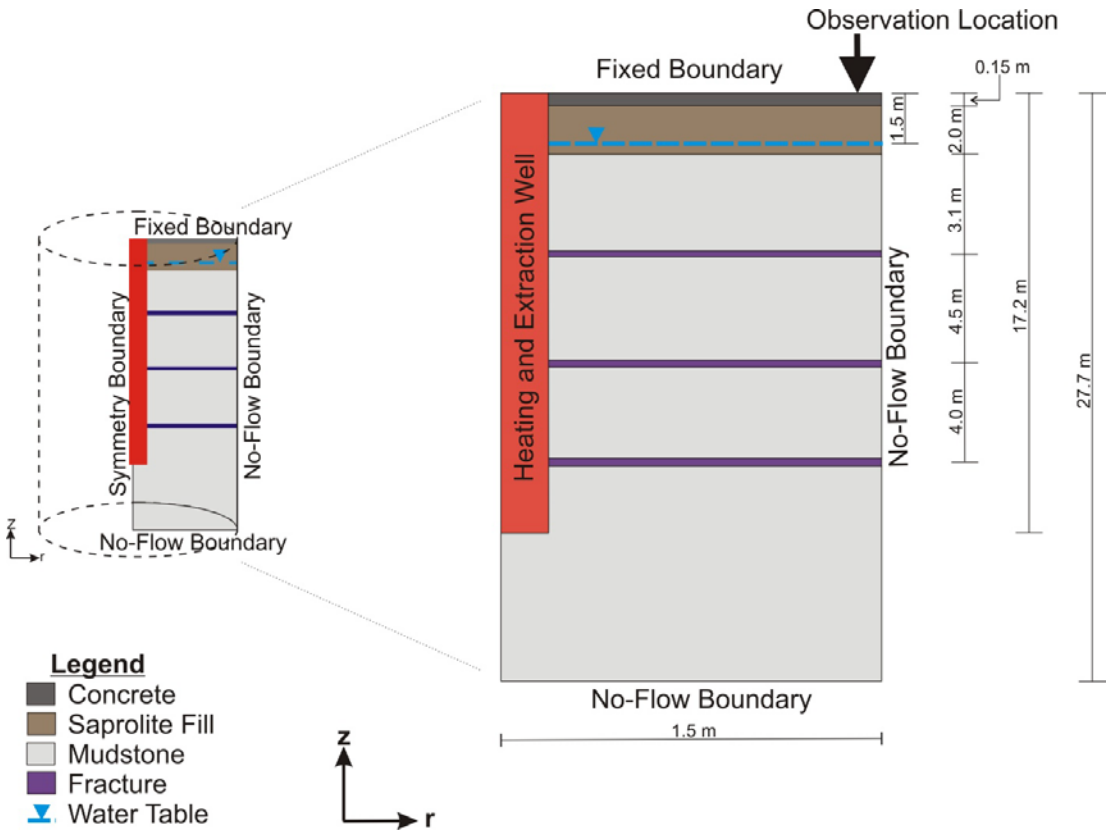

Figure 3-7 – Cross-sectional view of the conceptual 2D radial symmetric model.

The top boundary was fixed with a constant temperature of 10 °C and a constant pressure of 101,325 Pa representing atmospheric conditions while the bottom boundary was set to a no-flow boundary. The bottom boundary was extended 10.5 m below the treatment zone in order to reduce the influence of the bottom boundary condition on the model results. Before setting the bottom boundary to a no-flow boundary, a constant pressure of 356,231 Pa was applied and the model was run to steady state in order to create a water table approximately 1.5 m below the top of the model. One limitation of the radially symmetric domain is that a hydraulic gradient cannot be incorporated into the simulations. This presents ideal conditions as there was a hydraulic gradient observed during the pilot test.

Three horizontal fractures were incorporated into the model domain as illustrated in Figure 3-7. As discussed in Section 3.3.1, the bedrock underlying the NAWC site is composed of dipping layers of highly weathered and variably fractured rock. Dipping fractures could not be incorporated into the model domain due to the finite element grid selection as well as being radially symmetrical. The three fracture locations were selected based on the sharp spikes in TCE concentration found in the rock matrix pre-remediation samples as shown in Figure 3-4. The fracture zone cells had a 1 cm thickness and were assigned a permeability calculated according to the following depth-weighted arithmetic mean (Baston et al., 2010):

$$k_{fz} = \frac{k_f(e) + k_m(z_{fz} - e)}{z_{fz}} \tag{3.1}$$

where k_{fz} is the permeability assigned to the fracture zone cells, k_f is the fracture permeability calculated as $e^2/12$, e is the fracture hydraulic aperture assumed to be equal to the mechanical aperture, k_m is the matrix permeability, and z_{fz} is the thickness of the fracture zone cell (1 cm).

The fracture hydraulic aperture was calculated on the basis of hydraulic testing completed at the site by TerraTherm, Inc. in borings BR-1 through BR-3. A total of 32 hydraulic aperture values were calculated ranging from 54 microns to 234 microns with an arithmetic mean value of 138 microns. The average aperture was used in Equation 3.1 to calculate the permeability of the fracture zone cells and assigned to each of the three fractures in the model domain. A matrix permeability of $1.0x10^{-17}$ m^2 was assigned to the mudstone, which represents the arithmetic mean of two measurements performed on rock disks cut from pre-remediation rock core obtained from within the treatment zone. The resulting fracture zone permeability is calculated to be $1.0x10^{-11}$ m^2.

The TCE profile used as the baseline concentration for the model simulations was based on the average of the pre-remediation rock matrix concentrations measured during the pilot test in BR-1, BR-2 and BR-3.

3.3.3 Baseline Model Establishment

The primary objective of the numerical simulations was to compare rock matrix TCE mass removal achieved during the pilot test to that predicted by the model when subjected to similar heating conditions (i.e. temperature history). The average temperature recorded at measurement points T1 through T8 during the pilot test were matched by adjusting the daily energy input into the model. The matrix permeability was initially set to $1x10^{-17}$ m^2 and the fracture zone permeability set to $1x10^{-11}$ m^2 to match the average temperature profile.

Once the temperature profile was calibrated, the percentage of mass removal from the rock matrix was estimated to be 54% which is less than the average TCE removal measured during the pilot test at 63.5%. The pilot test at the NAWC site was conducted in a highly fractured, weathered grey mudstone which would allow for liquid and vapour extraction through the fracture network.

The model domain incorporated three fractures without vertical connections, as it assumes competent bedrock matrix in between the fractures. To better simulate the subsurface conditions within the pilot test zone (that likely contained several interconnected micro-fractures creating additional pathways for vapour extraction), a sensitivity analysis was completed using a range of matrix permeability values from $1x10^{-13}$ m^2 to $1x10^{-17}$ m^2. When changing the matrix permeability from $1x10^{-13}$ m^2 to $1x10^{-17}$ m^2 the average temperature in the model at the observation location varied by approximately 4 degrees. The greater the matrix permeability the lower the average temperature profile. This is shown in Figure 3-8. The permeability of the fracture zone cells was not recalculated using the equations above when the model matrix permeability was varied.

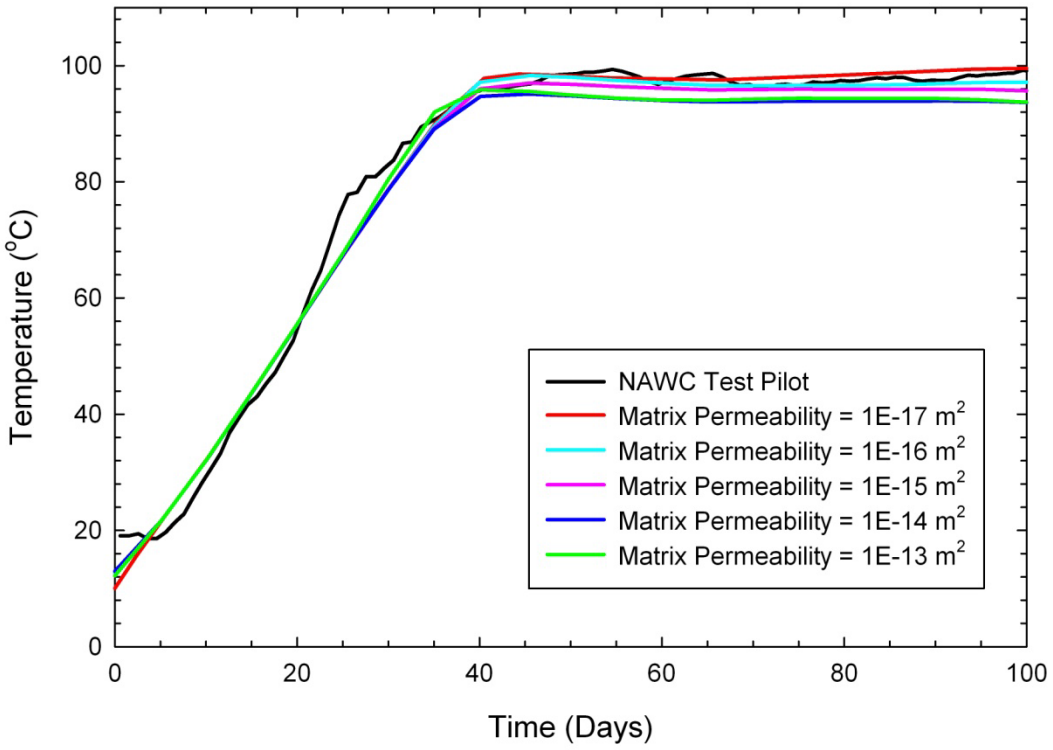

Figure 3-8 - Temperature versus time curve displaying the influence of matrix permeability.

The resulting percentage of TCE removed from the rock matrix during the various permeability simulations is displayed Table 3-1. This table shows that the percentage of TCE removed is greatest when the matrix permeability is set to $1x10^{-15}$ m^2, which had a 67% removal as compared to the pilot test of 63.5%. The model bulk permeability was calculated using the depth weighted arithmetic mean of the model matrix permeability and the model fracture permeability. When the model matrix permeability was set to $1x10^{-15}$ m^2, the model bulk permeability was calculated to be $3.5x10^{-14}$ m^2 which is comparible to the bulk permeability measured during hydraulic testing completed by TerraTherm Inc. in 2009 (a value of $8.4x10^{-14}$ m^2 was estimated).

Table 3-1 – Matrix bulk permeability of the numerical simulations with different matrix permeabilities applied.

Model Matrix Permeability (m^2)	Model Fracture Permeability (m^2)	Model Bulk Permeability (m^2)	Percent TCE Removed (%)
$1x10^{-17}$	$1.0x10^{-11}$	$2.0x10^{-14}$	54
$1x10^{-16}$	$1.0x10^{-11}$	$2.1x10^{-14}$	54
$1x10^{-15}$	$1.0x10^{-11}$	$3.5x10^{-14}$	67
$1x10^{-14}$	$1.0x10^{-11}$	$1.7x10^{-13}$	39
$1x10^{-13}$	$1.0x10^{-11}$	$1.5x10^{-12}$	42

Intuitively, the greatest amount of extraction was anticipated to occur with the highest matrix permeability of $1x10^{-13}$ m^2, but this was not the case. The primary route of TCE extraction occurs in the three fractures. Closer examination of the TCE concentrations at different time steps was completed with the matrix permeability set to $1x10^{-15}$ m^2 and $1x10^{-13}$ m^2.

Figure 3-9 displays the model-predicted TCE profile in the rock matrix at the observation location over time with a matrix permeability of $1x10^{-15}$ m^2. This figure shows that as the temperature in the rock matrix increases, boiling begins to occur in the fractures. At 30 days the matrix temperature was an average of 80 °C (prior to boiling) and the TCE concentration in the fracture

zone increased by 2 to 8 times greater than the initial concentration. This increase is a result of the TCE partitioning to the vapour phase in the small fracture zone areas. This phenomenon has been observed by Chen et al. (2010) during rock core laboratory experiments when boiling occurred in the rock core.

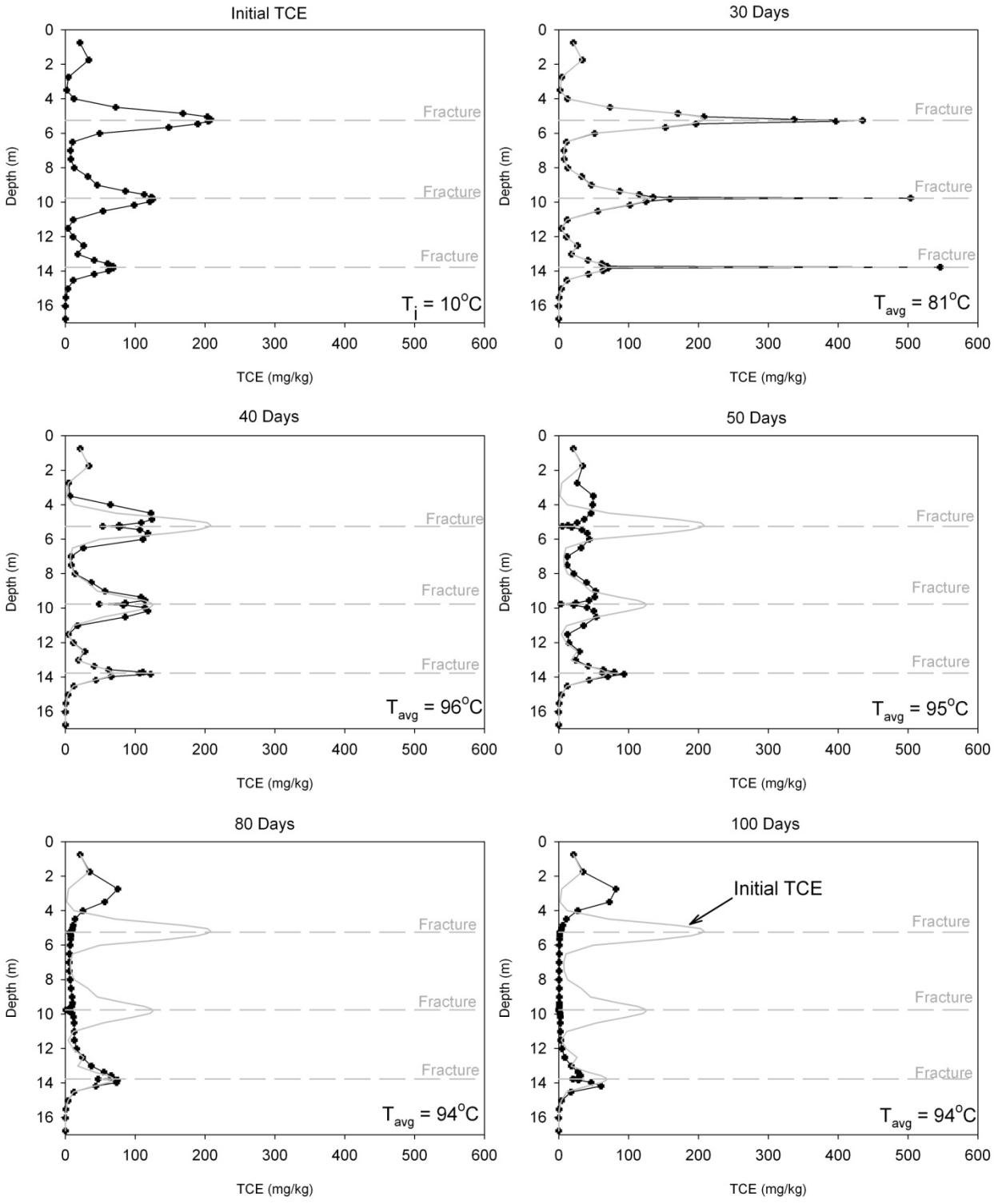

Figure 3-9 - Model-predicted TCE profile in the rock matrix at the observation location over time when the matrix permeability is set to $1x10^{-15}$ m^2. Grey curves represent the initial TCE concentration specified in the model.

The TCE concentration reduces primarily in the fracture zone cells of the upper two fractures after heating for 40 days due to extraction of the TCE vapours and liquids. Once heating of the matrix has occurred for 50 days, extraction is taking place in all three fractures. The concentration above the upper fracture begins to increase in concentration. By 80 days the TCE concentration between the top and bottom fracture is significantly decreased, but the concentration above the top fracture has increased in concentration. Once 100 days of heating has occurred (the end of the numerical simulation), the TCE profile shows that the TCE concentration above the upper fracture has increased. The TCE below the bottom fracture shifted its location slightly downward with the final concentration remaining nearly the same as the initial concentration in the bottom fracture. This shift in concentration was observed when the matrix permeability was set to $1x10^{-13}$ m^2 as discussed below.

Figure 3-10 shows the model-predicted TCE profile in the rock matrix, at the observation location over time, when the matrix permeability is set to $1x10^{-13}$ m^2. Boiling begins to occur in the model after 30 days of heating. Because the matrix permeability is only 2 orders of magnitude smaller than the fracture zone permeability ($1x10^{-11}$ m^2), the TCE partitions into the vapour phase not only in the fracture zone cells, but also in the matrix. The TCE mobilized differently than previously observed. The concentration increased in the area above the uppermost fracture and in between the uppermost and middle fractures.

At 40 days, boiling continues and the TCE vapour in between the uppermost fracture and bottom fracture are extracted, therefore creating a significant concentration decrease in the matrix. TCE vapour migrates to above and below the fracture zone creating an increase in concentration. As the simulation continues to 100 days, the concentration above the top fracture decreased slightly, but the TCE continues to migrate deeper into the rock matrix below the bottom fracture.

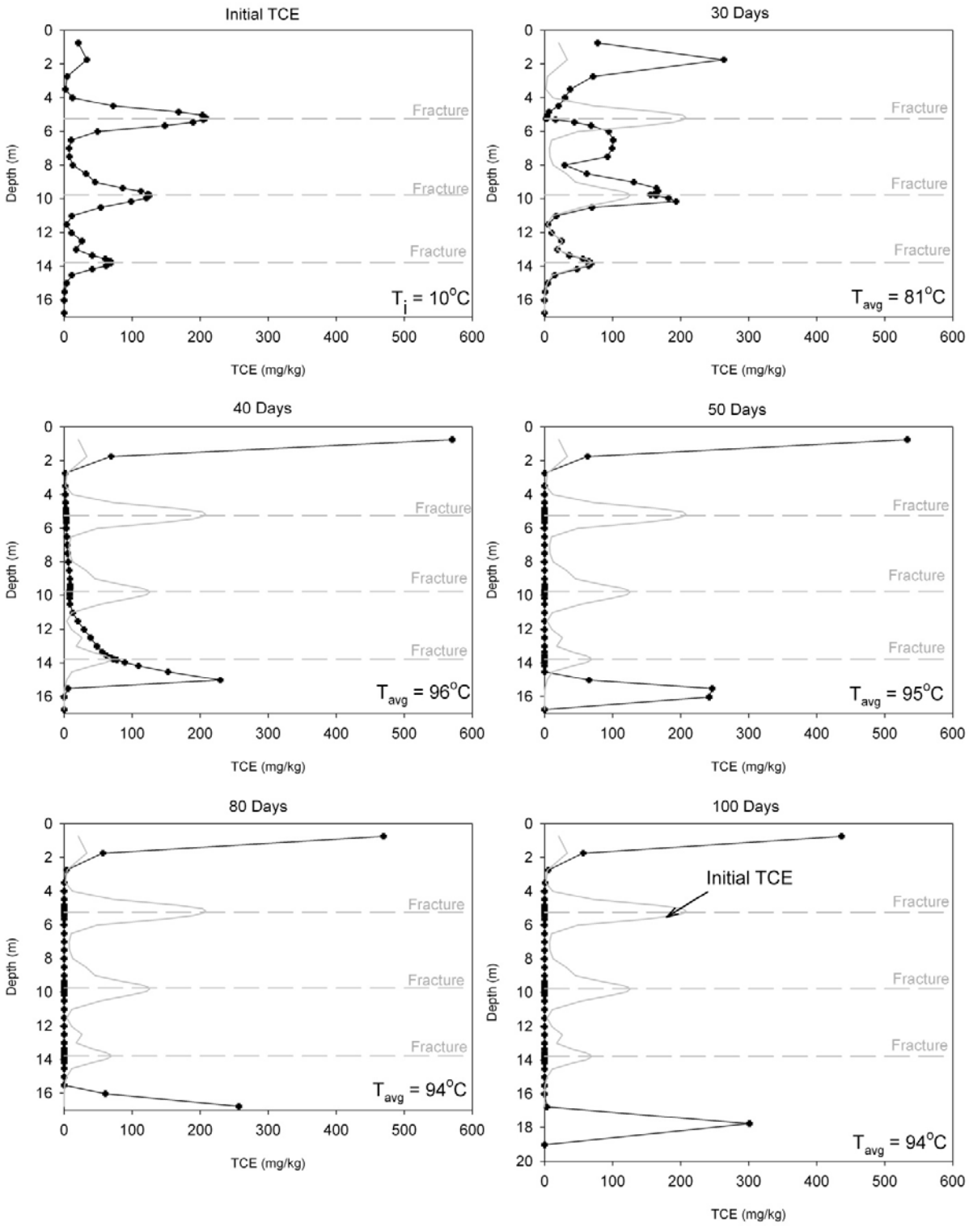

Figure 3-10 - Model-predicted TCE profile in the rock matrix at the observation location over time when the matrix permeability is set to $1x10^{-13}$ m^2. Grey curves represent the initial TCE concentration specified in the model.

Figures 3-9 and 3-10 demonstrate that as the rock matrix permeability is increased, becoming closer in magnitude to the value of the fracture zone permeability, the TCE is able to mobilize beyond the fracture zone cells. This occurs due to the pressure gradients that are formed when the permeability is altered. Figure 3-11 displays the pressure profiles at the observation location for the two different scenarios discussed above.

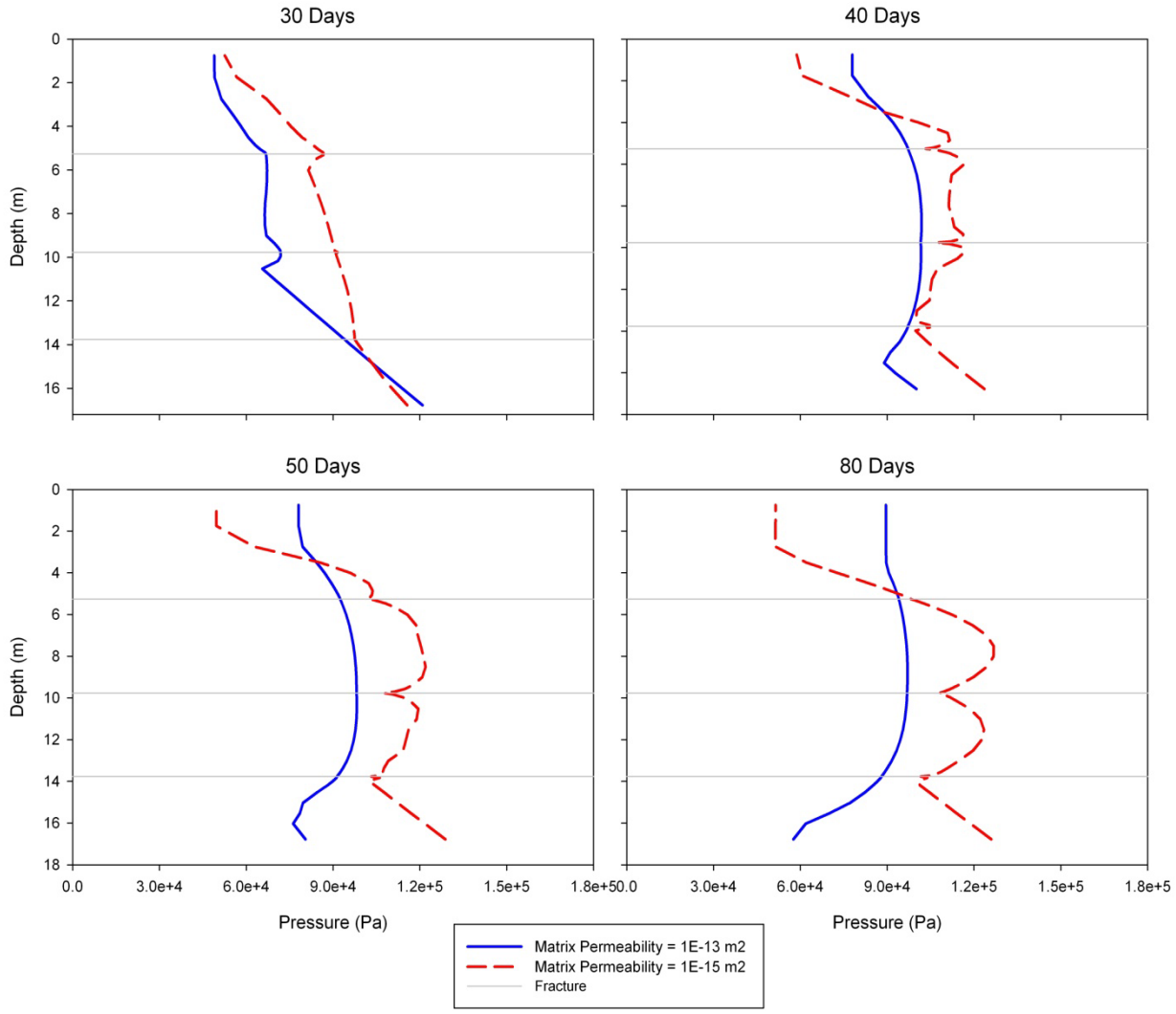

Figure 3-11 – Model-predicted pressure profiles at the observation location when the matrix permeability is set to $1x10^{-13}$ m^2 and $1x10^{-15}$ m^2.

As previously discussed, the primary route of TCE extraction is through the fracture zone cells. When the temperature in the rock matrix is increased, the pressure is also increased. For all time steps shown in Figure 3-11 when the matrix permeability is set to $1x10^{-13}$ m^2 (therefore closer in magnitude to the fracture zone cells), the pressure distribution is relatively constant between the fracture zone cells and the matrix. There is a pressure decrease towards the fill and saprolite layer as well as towards the bottom of the heating zone.

When the permeability is decreased ($1x10^{-15}$ m^2), pressure gradients are formed towards the fracture zone areas except for above the top fracture where the pressure gradient is driven towards the higher permeability fill area.

These pressure gradients dictate the redistribution of TCE seen in Figures 3-9 and 3-10. When the TCE is vapourized it is driven by the pressure gradients and will migrate from a high pressure area to a low pressure area. When the matrix permeability is $1x10^{-13}$ m^2, there is no significant pressure gradient towards the fracture zone cells but instead above and below the fracture area and thus there was redistribution of TCE above and below the fractures. When the permeability is set to $1x10^{-15}$ m^2, there are 4 orders of magnitude different between the fracture zone cells and the matrix therefore the pressure gradients are created and the TCE vapours travel from the higher pressures in the matrix to the lower pressures in the fracture zone where it is ultimately removed. Because of the higher permeability fill layer above the fracture area, there is a gradient created towards the fill and hence some TCE migration to the zone above the uppermost fracture.

From this sensitivity analysis, it can be concluded that the optimal matrix permeability was $1x10^{-15}$ m^2 as it has the greatest percentage of TCE removed from the rock matrix and did not cause significant redistribution of the TCE above and below the heating zone. For these reasons, a

matrix permeability of $1x10^{-15}$ m^2 was used for the baseline model simulation to complete the sensitivity analysis discussed in Section 3.3.4.

The model simulations represent an idealized scenario by having three primary fractures. Increasing the matrix permeability helps to account for the possible fracture networks in the subsurface at the NAWC site. The simulations clearly demonstrate that the primary pathway for TCE removal is through the fracture zone cells and when the matrix permeability becomes close to the fracture zone permeability the driving force (the pressure) towards the fractures is significantly decreased.

A summary of the baseline model input parameters used for the sensitivity analysis discussed in Section 3.3 is provided in Table 3-2. Thermal conductivity, specific heat capacity, pore compressibility and the Klinkenberg parameter were assumed to be equal for the saprolite and bedrock. Scaled power functions were used by TMVOC to calculate the gas and liquid water phase relative permeabilities following Stone (1970). The capillary pressure functions were adapted from Falta et al. (1992), which were calculated using modified versions of the van Genuchten (1980) constitutive model given by Parker et al. (1987). The total mass of TCE removed from the rock matrix during the pilot test was estimated to be 63.5% of the initial amount (Rodriguez et al., 2012). The calibrated baseline model predicted 67% TCE mass removal.

Table 3-2 – Baseline model input parameters.

Parameter	Units	Saprolite	Mudstone Bedrock	Fracture Zone Cells
Density	kg/m^3	2520	2520	2520
Permeability	m^2	$6.5x10^{-13}$	$1.0x10^{-15}$	$1.0x10^{-11}$
Porosity[1]	%	30	3.3	3.3
C_{wet} [2]	W/m°C	2.84	2.84	2.84
C_{dry} [2]	W/m°C	2.19	2.19	2.19
Specific heat capacity[3]	J/kg°C	1000	1000	1000
Pore compressibility[4]	Pa^{-1}	$3.0x10^{-9}$	$3.0x10^{-9}$	$3.0x10^{-9}$
Klinkenberg parameter[5]	Pa^{-1}	$2.4x10^{-6}$	$2.4x10^{-6}$	$2.4x10^{-6}$
Fraction organic carbon	-	0.0079	0.0079	0.00

1. The saprolite layers were assumed to have a porosity of 30% which is a common porosity for silts and clays as specified by Hough (1957).
2. C_{wet} is the thermal conductivity under saturated conditions and C_{dry} is the thermal conductivity under de-saturated conditions. This parameter was calculated using the equations in Woodside and Messmer (1961) with a thermal conductivity of the matrix of 3.0 W/m°C.
3. Schärli and Rybach (2001); Čermák and Rybach (1982).
4. Zimmerman (1991).
5. Webb and Pruess (2003).

3.3.4 Sensitivity Analysis Outline

The baseline calibrated model was used to perform a sensitivity analysis to examine what parameters are most influential in dictating the amount of TCE mass removal from the rock matrix. Table 3-3 summarizes the parameters that were varied in addition to the matrix permeability in the sensitivity analysis and the range of values that were considered.

Table 3-3 – Sensitivity analysis parameters.

Parameter	Unit	Baseline Model	Values Considered
Field Parameters			
Permeability	m^2	$1x10^{-15}$	10^{-17}, 10^{-16}, 10^{-14}, 10^{-13}
Matrix Porosity	%	3.3	1, 5, 10
Thermal Conductive Heating Parameter			
Energy Rate	J/s	Field Temperature Match	-10%, +10%, +20%, +30%

3.4 Sensitivity Results and Discussion

3.4.1 Matrix Porosity

Primary porosity is created when the rock is formed and is referred to here as the matrix porosity; secondary porosity is created due to geological processes such as weathering and fracturing (Singhal and Gupta, 1999). The 2D simulations only considered primary porosity with the baseline model having a matrix porosity of 3.3%, which was determined through laboratory testing on core samples obtained from within the target heating zone.

Figure 3-11 displays the model-predicted temperature-time curves when the matrix porosity is altered between 1 and 10%. Figure 3-12 displays the percentage of TCE removed as a function of matrix porosity. Figures 3-11 and 3-12 illustrate that the matrix porosity does not significantly affect the temperature of the rock matrix when the same amount of energy is applied in the numerical model. However, the matrix porosity does influence the percentage of TCE removed from the rock matrix. As the porosity increases, the TCE removed at 100 days also increases. There was 10% more TCE removed from the rock matrix when the matrix porosity was increased from 3.3% to 10%.

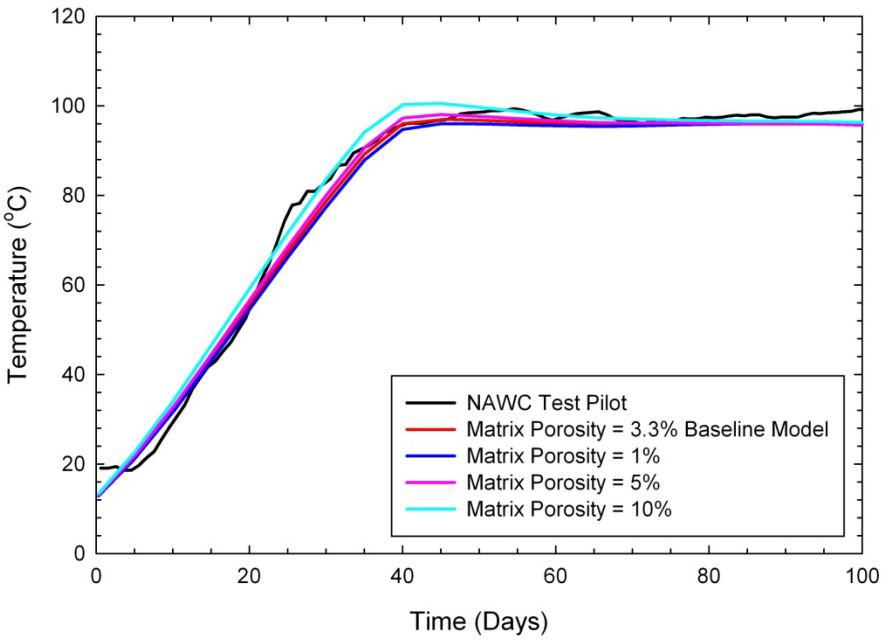

Figure 3-12 - Temperature versus time curve displaying the influence of matrix porosity.

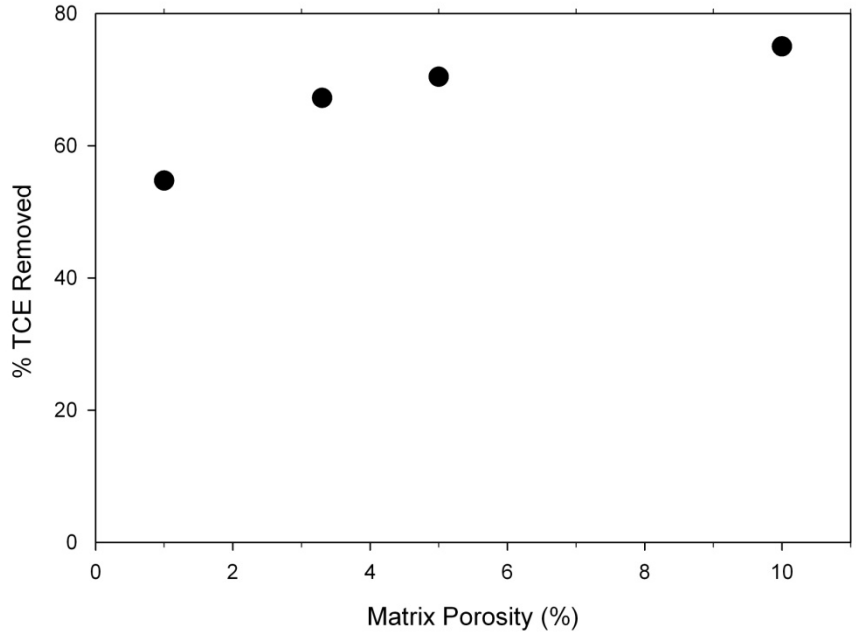

Figure 3-13 - Percentage of TCE removed from the rock matrix at 100 days when the matrix porosity is varied from 1 to 10%.

3.4.2 Energy Rate

A variable energy rate (J/s) was applied to the column of matrix blocks where the heater/extraction well was located on the inner radius of the model domain. A higher energy was applied until the maximum average temperature was reached in which the energy was then reduced to sustain that temperature. The baseline model had an energy input that created a temperature-time profile similar to what was recorded during the NAWC pilot test. This energy was then increased or decreased to examine what effects the energy input into the rock matrix has on TCE removal.

The baseline model energy input was varied from a 10% decrease in energy to a 30% increase in energy, as shown in Figure 3-13. When the temperature in the rock matrix is increased by increasing the energy input, the percentage of TCE removed is also increased (Figure 3-14). A decrease in energy rate by 10% reduces the temperature to near the boiling temperature of TCE and this resulted in 20% of TCE being removed from the rock matrix.

When a 30% increase in energy input is applied, the maximum temperature achieved in the rock matrix was 112 °C and 86% of the TCE removed. While, when a 20% increase in energy was applied it resulted in 84.5% TCE removal. It can be concluded from this study that a greater energy into the rock matrix results in higher maximum temperatures reached in the model but there is little final benefit to increasing the energy input to more than 20% as the final contaminant removal after 100 days between 20% and 30% was insignificant.

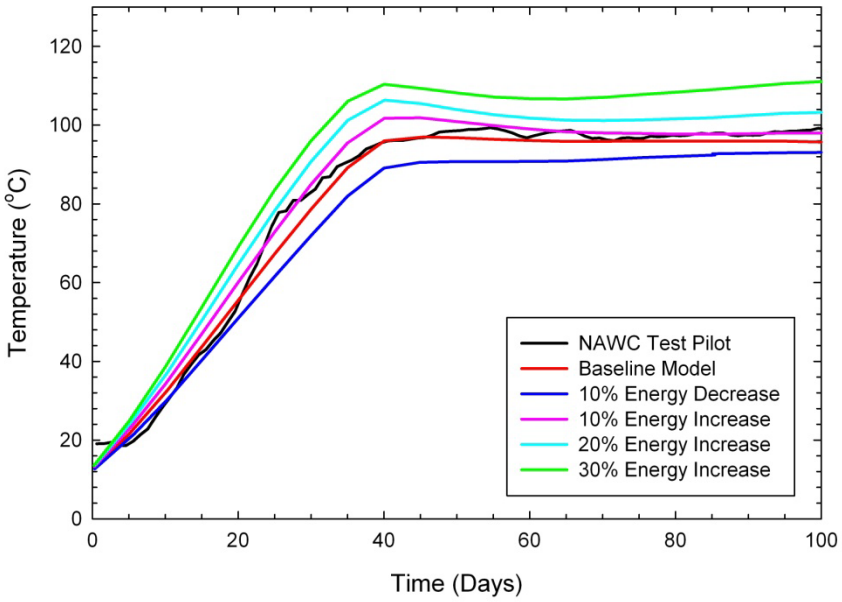

Figure 3-14 - Temperature versus time curve displaying the influence of a change in energy input to the rock matrix.

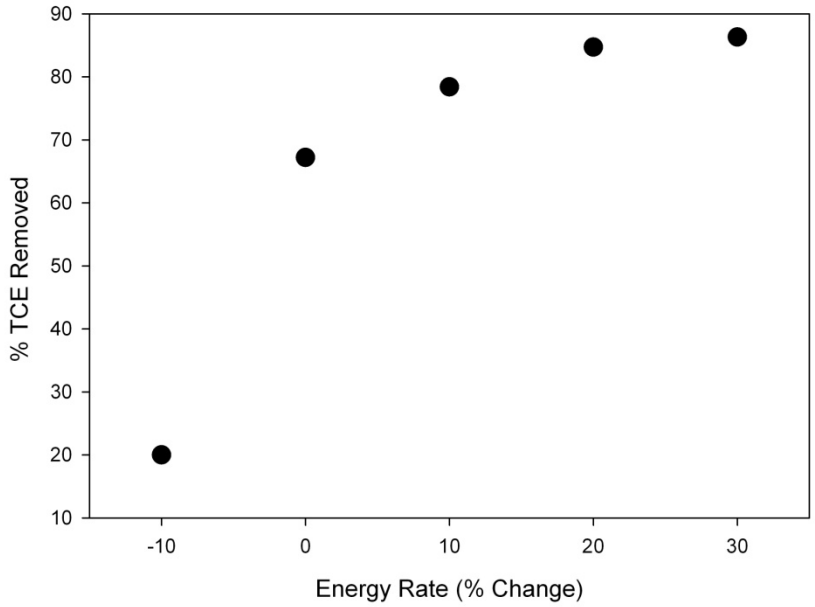

Figure 3-15 - Percentage of TCE removed from the rock matrix at 100 days when the energy input into the 2D simulations is varied.

3.5 Conclusions

A thermal conductive heating field pilot test was conducted in 2009 at the Naval Air Warfare Center in West Trenton, New Jersey in which historical TCE contamination is found in fractured mudstone bedrock. The pilot test consisted of a network of 15 heater/extraction wells that were operated for 102 days to remove TCE from the rock matrix. Using the data collected at the site, a 2D screening model was created using TMVOC in which the primary objective was to examine the TCE mass removal in the rock matrix from the numerical simulations compared to the pilot test.

The pilot test was found to have a TCE removal in the rock matrix of 63.5% as compared to the baseline model simulation which had a removal of 67%. The numerical model presented ideal conditions, such as only 3 fractures separated by competent bedrock and no hydraulic gradient. A sensitivity analysis on the rock matrix permeability was conducted to calibrate the model with the field results. It was concluded that for the numerical simulations a matrix permeability of $1x10^{-15}$ m^2 was appropriate due to the idealized model conditions. The fracture zone cells were identified to be the primary area where TCE removal occurred due to the higher permeability in these cells compared to the lower permeability in the rock matrix. The sensitivity analysis concluded that the greater the maximum temperature sustained in the model, the greater the percentage of TCE removed from the rock matrix.

Future investigations using numerical simulations could create a model with a more realistic fracture network in the subsurface rather than ideal conditions. Creating a 3-dimensional model rather than a radially symmetric model would also allow for a hydraulic gradient to be applied to the model. Using a 2D model does not account for the heating influence of nearby wells, therefore creating a 3D model would also allow for these interactions to be observed. Heating

well interactions could also increase the subsurface temperatures therefore resulting in greater TCE removal from the rock matrix.

3.6 Acknowledgements

The authors of this manuscript would like to thank the U.S. Department of Defense (DoD) Environmental Security Technology Certification Program (Project ER-0715) and Queen's University for financial support of this work. Thank you to TerraTherm Inc., the United States Geological Survey (USGS), and the US Navy for their collaboration on this project.

3.7 Literature Cited

Baker, R.S. & Kuhlman, K. 2002. *A Description of the Mechanisms of In-Situ Thermal Destruction (ISTD) Reactions*. In: H. Al-Ekabi (Ed.), Current Practices in Oxidation and Reduction Technologies for Soil and Groundwater, Presented at the 2nd International Conference on Oxidation and Remediation Technologies for Soil and Groundwater, ORTs-2, Toronto, Ontario, Canada, Nov. 17-21, 2002.

Baston, D.P., Falta, R.W., & Kueper, B.H. 2010. *Numerical Modeling of Thermal Conductive Heating in Fractured Bedrock.* Ground Water 48: 836-843.

Baston, D.P. & Kueper, B.H. 2009. *Thermal conductive heating in fractured bedrock: Screening calculations to assess the effect of groundwater influx.* Advances in Water Resources 32, 231-238.

Čermák, V., and Rybach, L. 1982. *Thermal conductivity and specific heat of minerals and rocks.* In G. Angenheister (Ed.) Landolt-Börnstein: Numerical Data and Functional Relationships in Science and Tehcnology, Group V (Geophysics and Space Research), Volume 1a (Physical Properties of Rocks), (pp. 305{343). Springer, Berlin-Heidelberg.

Chen, F., Xiaoling, L., Falta, R.W., and Murdoch, L.C. 2010. *Experimental Demonstration of Contaminant Removal from Fractured Rock by Boiling.* Environmental Science & Technology 44: 6437-6442.

Falta, R.W., Pruess, K., Javandel, I., and Witherspoon, P.A. 1992. *Numerical Model of Steam Injection for the Removal of Nonaqueous Phase Liquids From the Subsurface: 2. Code Validation and Application.* Water Resources Research 28: 451-465.

Heron, G., Parker, K., Galligan, J., and Holmes, T.C. 2009. *Thermal Treatment of Eight CVOC Source Zones to Near Nondetect Concentrations.* Ground Water Monitoring and Remediation 29: 56-65.

Hough, B.K. 1957. *Basic Soils Engineering.* Ronald Press Co., New York.

Johnson, P., Dahlen, P., Triplett, J., Foote, E., and Williams, S. 2009. State-*of-the-Practice Overview: Critical Evaluation of State-of-the-Art In Situ Thermal Treatment Technologies for DNAPL Source Zone Treatment*. ESTCP Project ER-0314.

Lacombe, P.J., & Burton, W.C. 2010. *Hydraulic Framework of Fractured Sedimentary Rock, Newark Basin, New Jersey*. Ground Water Monitoring & Remediation 30: 35-45.

Lewis-Brown, J.C., Carleton, G.B., and Imbrigiotta, T.E. 2006. *Hydraulic and Solute-Transport Properties and Simulated Advective Transport of Contaminated Ground Water in a Fractured-Rock Aquifer at the Naval Air Warfare Center, West Trenton, New Jersey, 2003.* U.S. Geological Survey, Scientific Investigations Report 2005-5049.

Parker, J.C., Lenhard, R.J., and Kuppusamy, T. 1987. *A parametric model for constitutive properties governing multiphase flow in porous media.* Water Resources Research 23: 618-624.

Pruess, K., & Battistelli, A. 2002. *TMVOC, A Numerical Simulator for Three-Phase Non-isothermal Flows of Multicomponent Hydrocarbon Mixtures in Saturated-Unsaturated Heterogeneous Media.* Lawrence Berkeley National Laboratory, Berkeley, CA.

Rodriguez, D.J., and Kueper, B.H. 2012. *Assessment of Thermal Conductive Heating for the Remediation of DNAPL Contaminated Fractured Bedrock.* (In Progress).

Schärli, U., and Rybach, L. 2001. *Determination of specific heat capacity on rock fragments.* Geothermics 30: 93-110.

Singhal, B.B.S., & Gupta, R.P. 1999. *Applied Hydrogeology of Fractured Rocks.* Kluwer Academic Press, Netherlands.

Stone, H.L. 1970. *Probability Model for Estimating Three-Phase Relative Permeability.* Journal of Petroleum Technology February: 214-218.

Tiedeman, C.R., Lacombe, P.J., and Goode, D.J. 2010. *Multiple Well-Shutdown Test and Site-Scale Flow Simulation in Fractured Rocks.* Ground Water, 45(3):May-June 401-415.

Triplett Kingston, J.L., Dahlen, P.R., & Johnson, P.C. 2010. *State-of-the-Practice Review of In Situ Thermal Technologies.* Ground Water Monitoring & Remediation 30, 64-72.

van Genuchten, M.T. 1980. *A closed-form equation for predicting the hydraulic conductivity of unsaturated soils.* Soil Science Society of America Journal 44: 892-898.

Woodside, W., and Messmer, J. 1961. *Thermal conductivity of porous media*. Journal of Applied Physics, 32: 1688-1706.

Webb, S.W., and Pruess, K. 2003. *The Use of Fick's Law for Modeling Trace Gas Diffusion in Porous Media.* Transport in Porous Media 51: 327-341.

Zimmerman, R.W. 1991. *Compressibility of sandstones*, Developments in Petroleum Science 29, Elsevier, New York, NY, USA.

Chapter 4

Conclusions and Recommendations

In 2009 a pilot test was conducted at the Naval Air Warfare Center in West Trenton, New Jersey which employed thermal conductive heating. The site is historically contaminated with trichloroethylene in the mudstone bedrock. The pilot test was completed on a small portion of the site with an area of 45.6 m^2. A network of 15 heater/extraction wells that conducted vapour and liquid extraction was installed to a depth of 16.8 m below the ground surface. Each well was screened to allow for maximum extraction of fluids and the pilot test was conducted over 102 days.

Using the data collected during the pilot test, a two-dimensional numerical model was created using TMVOC which is part of the TOUGH2 family of codes that is capable of simulating multiphase flow, heat transfer, and transport of volatile organic compounds. The primary objective was to create a screening model in order to examine the TCE mass removal from the rock matrix in the numerical summations compared to the pilot test.

Three rock core samples were taken pre- and post-remediation during the pilot test at the NAWC site. The core samples were measured for TCE concentrations before and after heating to measure the percentage of mass removed from the rock matrix. The pilot test resulted in an average of 63.5% TCE removal after 102 days. The two-dimensional radial finite difference model simulations were designed to simulate the heater/extraction well that was located in the center of the well network during the pilot test. The simulations contained three primary fracture zone locations which were selected based upon the pre-remediation rock core TCE concentration findings with competent bedrock in between. Temperature data collected during the pilot test was

used in the numerical simulations to match the heating patterns observed. The baseline model had a 67% TCE removal from the rock matrix after 100 days of heating which was similar to that measured during the pilot test.

The numerical model presents ideal conditions as it only contained three fractures separated by competent bedrock. As it was a radially symmetric model no hydraulic gradient can be incorporated. The pilot test was conducted in highly fractured weathered bedrock which most likely contained numerous fracture networks. To help account for this, the matrix permeability in the numerical simulations was increased. The simulations demonstrated that the primary pathway for extraction was through the three fracture zones in the model.

A limited sensitivity analysis was completed on the baseline simulation which also examine the effect that matrix porosity and energy input into the subsurface has on the effectiveness of the remedial system. The sensitivity analysis concluded that the greater the maximum temperature sustained in the model, the greater the percentage of TCE removed from the rock matrix. It also demonstrated that there was not a significant benefit (i.e. TCE removal) when a 30% increase in energy was applied to the model versus 20% for 100 days. The results from this study may help generate recommendations for future TCH remediation applications in fractured bedrock aquifers as the simulations demonstrated that the fracture zone plays an important role in the amount of contaminant removed from the rock matrix.

Future investigations using TMVOC could be completed to further examine the success of mass removal from fractured rock. Future investigations could include:

- Incorporating a fracture network in the subsurface rather than three primary fractures which account for vertical and horizontal connections.

- Creating a three-dimensional model rather than a radially symmetric model would allow for a hydraulic gradient to be applied to the model which may also affect the amount of contaminant removal from the subsurface.
- Incorporation the 15 heating/extraction wells into a 3D model domain in a similar layout as the pilot test. This would allow for the influence and interactions of the nearby wells in the well network which were not accounted for in the two-dimensional model to be examined.
- Conduct a sensitivity analysis on the horizontal and vertical grid discritization.
- Conduct a sensitivity analysis on the permeability of the fracture zone cells to examine if there is more TCE extraction with increased fracture zone permeability. This permeability could be varied using the range of fracture apertures calculated from the hydraulic testing during the pilot test.

.

Appendix A

TMVOC Governing Equations

This section provides a brief summary of the governing equations and assumptions that are used by TMVOC, A Numerical Simulator for Three-Phase Non-isothermal Flows in Multicomponent Hydrocarbon Mixtures in Saturated-Unsaturated Heterogeneous Media. Further information can be found in the TMVOC user manual by Pruess and Battistelli (2002).

TMVOC is a numerical model developed at the Lawrence Berkeley National Laboratory, which is capable of simulating three-dimensional heterogeneous porous media or fractured rock. It is an extension of the TOUGH2 simulator and considers multi-component volatile organic compound (VOC) flow in all three phases (gas-water-NAPL) above and below the groundwater table. TMVOC is able to simulate non-condensable gases as well as advection, dispersion, sorption, phase partitioning and biodegradation. TMVOC allows for irregular grids to be created by using the Integral Finite Difference Method (IFDM) for space discritization.

The structure and execution of TMVOC uses the same architecture as TOUGH2 (Figure A-1). Primary and secondary input variables are specified by the user for which the numerical model uses a series of linear equations and equations of state (EOS) modules to produce the output.

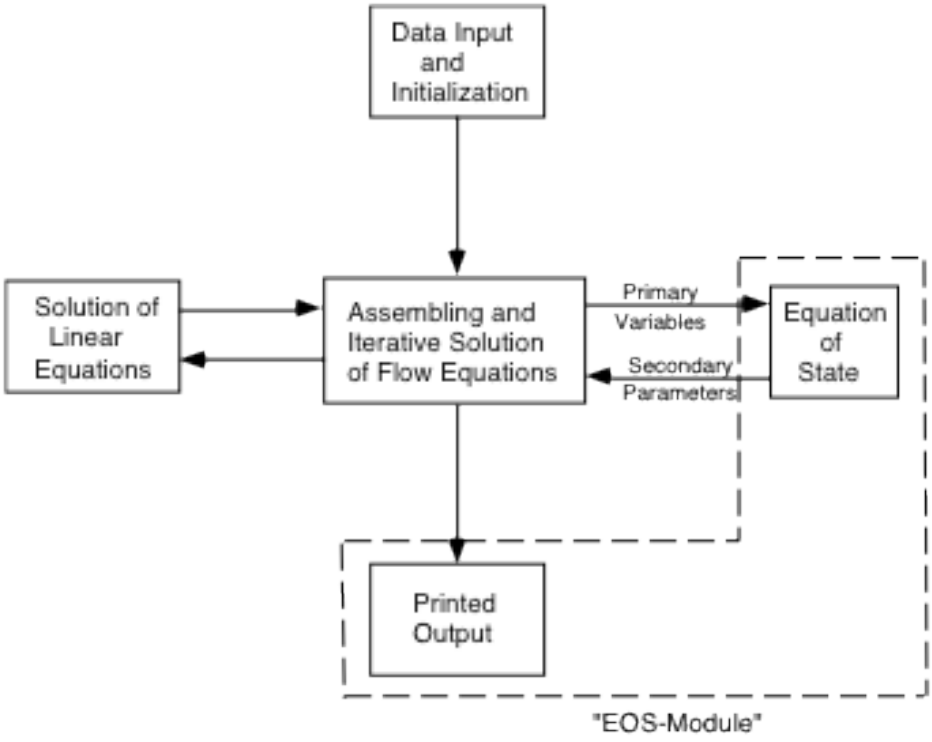

Figure A-1 – TMVOC architecture (Pruess and Battistelli, 2002).

TMVOC can simulate heat transfer applications such as thermal remediation and steam injection remediation technologies. Heat transfer simulated by TMVOC occurs by conduction and multi-phase convection. TMVOC assumes that the three phases are in "local chemical and thermal equilibrium".

Air and other non-condensable gases can be incorporated into the numerical simulator. If there are VOC vapors present in the system then Raoult's Law governs which is dependent on the aqueous phase concentration and vapor pressure for single component mixtures, which can be seen in Equation A.1.

$$x_g P_g = x_n P_{vap} \tag{A.1}$$

where x is the mole fraction of the chemical component in the gas (g) and the NAPL (n), and P is the pressure of the gas and the vapor pressure.

The aqueous phase is dominated by water. When VOCs are present, the composition of the water is dependent on the concentration in NAPL or gas phase and the solubility of the VOC. When non-condensable gases are present they are represented by TMVOC using Henry's Law.

The NAPL phase (oil phase) considers only VOCs and assumes that the solubility of water and non-condensable gases (NCGs) into the NAPL phase is minimal. The solubility of the NAPL in water follows the equation given by Hoot et al. (1957):

$$x_n^w = 0.281226 - 4.23610v + 1.75244v^2 \tag{A.2}$$

where,

$$v = \log_{10}(1.8T_c + 32) \tag{A.3}$$

and T_c is the temperature in degrees Celsius.

TMVOC uses a general mass and energy balance equation as follows:

$$\frac{d}{dt}\int_{V_n} M^\gamma dV_n = \int_{\Gamma_n} F^\gamma \cdot n d\Gamma_n + \int_{V_n} b^\gamma dV_n \tag{A.4}$$

where M is the mass accumulation term for the component γ (if β=1 it denotes water, NCGs or VOCs; or γ= NK + 1 to represent the heat component), and is integrated over a domain V_n. It is equal to the integral of the mass or heat flux, F, "bounded by the closed surface", Γ_n, plus the

integration of the sinks and sources, b. “n is a normal vector on surface element $d\Gamma_n$, pointing inward into V_n”.

The mass accumulation term is represented for the water and NCG components in the model by Equation A.5.

$$M^{\gamma} = \eta \sum_{\beta} S_{\beta} \rho_{\beta} x_{\beta}^{\gamma} \tag{A.5}$$

where γ can be the mass or heat component for the fluid phases β, which can be in a liquid, gas or NAPL state. η is the porosity, S is the saturation, ρ is the density and x is the mole fraction. The mass and heat accumulation formulas include rock properties such as sorption onto the rock grains (represented in second half of Equation A.6) and the specific heat of rock, C_R for the heat accumulation equation (Equation A.7).

$$M^{K} = \phi \sum_{\beta} S_{\beta} \rho_{\beta} x_{\beta}^{\gamma} + (1 - \phi) \rho_R \rho_w x_w^{\gamma} K_d \tag{A.6}$$

with ρ representing the density (of the phase, β, rock, R, or water, w) and K_d the distribution coefficient. The heat accumulation formula is as follows:

$$M^{NK+1} = (1 - \phi) \rho_R C_R T + \phi \sum_{\beta} S_{\beta} \rho_{\beta} u_{\beta} \tag{A.7}$$

where T is the temperature and u_{β} is the specific internal energy. The accumulation terms are discretized in space using the IFDM.

Literature Cited

Pruess, K., & Battistelli, A. 2002. *TMVOC, A Numerical Simulator for Three-Phase Non-isothermal Flows of Multicomponent Hydrocarbon Mixtures in Saturated-Unsaturated Heterogeneous Media.* Lawrence Berkeley National Laboratory, Berkeley, CA.

Appendix B

Model Testing

When using an existing numerical model, it is important to determine if it has been correctly compiled. To determine that TMVOC was compiled correctly, Example Problem 5 from the document entitled "TMVOC, A Numerical Simulator for Three-Phase Non-isothermal Flows of Multicomponent Hydrocarbon Mixtures in Saturated-Unsaturated Heterogeneous Media" written by Pruess and Battistelli (2002) was used and is further referred to as the TMVOC Users Manual. The TMVOC Users Manual provides a copy of the input files which can be used directly to run the simulations. This example was selected because it not only contained input files which could be used to run the simulations, but several graphed figures that could be re-generated for comparison to verify the model was compiled correctly.

Example Problem 5 simulates a laboratory experiment conducted by Hunt et al. (1988) which was "designed to evaluate the mobilization and transport of a [non aqueous phase liquid (NAPL)] during water and steam flooding" (Falta et al., 1992). The simulation modeled a 91 cm horizontal laboratory column with a cross sectional area of 20.428 cm^2 and examines the displacement of a benzene-toluene mixture during waterflooding. The model consisted of 50 evenly space elements filled with sand which had a density of 2650 kg/m^3, a porosity of 38.5% and a permeability of $1.6x10^{-11}$ m^2. The first part of the simulation was to inject the benzene-toluene mixture into the 15^{th} element (approximately 27 cm from the inlet) at a constant rate into the column over a 120 second period. Figure B-1 shows the conceptual model of the laboratory experiment and model simulations (Falta et al, 1992).

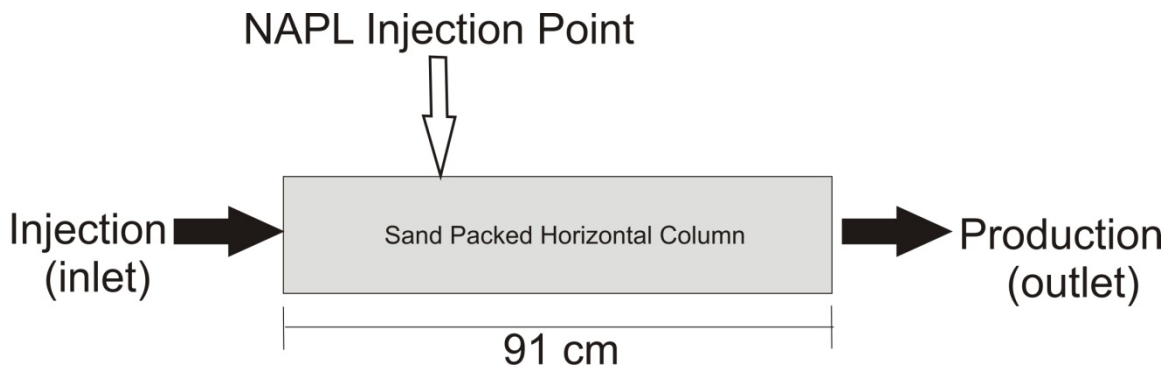

Figure B-1 – Conceptual diagram of the model simulations (Falta et al., 1992).

The second step of the simulation was to induce a waterflood into the horizontal column. Waterflooding is a process by which water at 22 °C is injected into the left side of the horizontal column and allowed to flow through the column and drain out the opposite side. The simulation injected 10.2 pore volumes (PV) of water into the column for the waterflood.

Figure B-2 below shows the non aqueous phase liquid (NAPL) saturations along the 91 cm horizontal column distance. The figure displays the NAPL saturation before waterflood which is part 1 of the simulation when the benzene-toluene mixture was injected for 120 s. The waterflood occurred for the second part of the simulation and the NAPL saturation of the benzene-toluene mixture was shown for 2,422 seconds which corresponds to 1.2 pore volumes (PV), 18,162 seconds (9 PV) and 108, 971 s (10.2 PV).

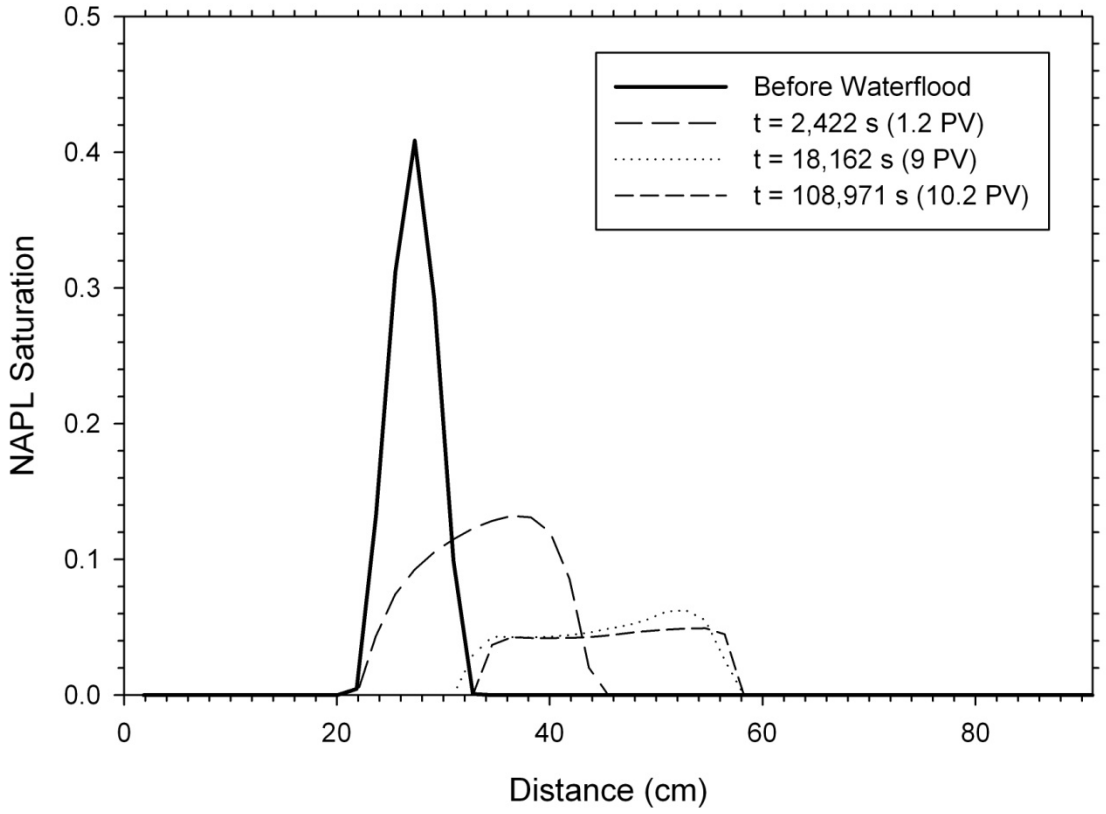

Figure B-2 – Re-created Figure 10.5.5 from the TMVOC Users Manual, Example Problem No. 5 to demonstrate model calibration.

To further examine if calibration of TMVOC was correct, Figure 10.5.6 from Example Problem 5 in the TMVOC Users Manual was recreated and is shown in Figure B-3. Figure B-3 displays the benzene and toluene aqueous mass fractions over time at the horizontal column outlet (at 91 cm).

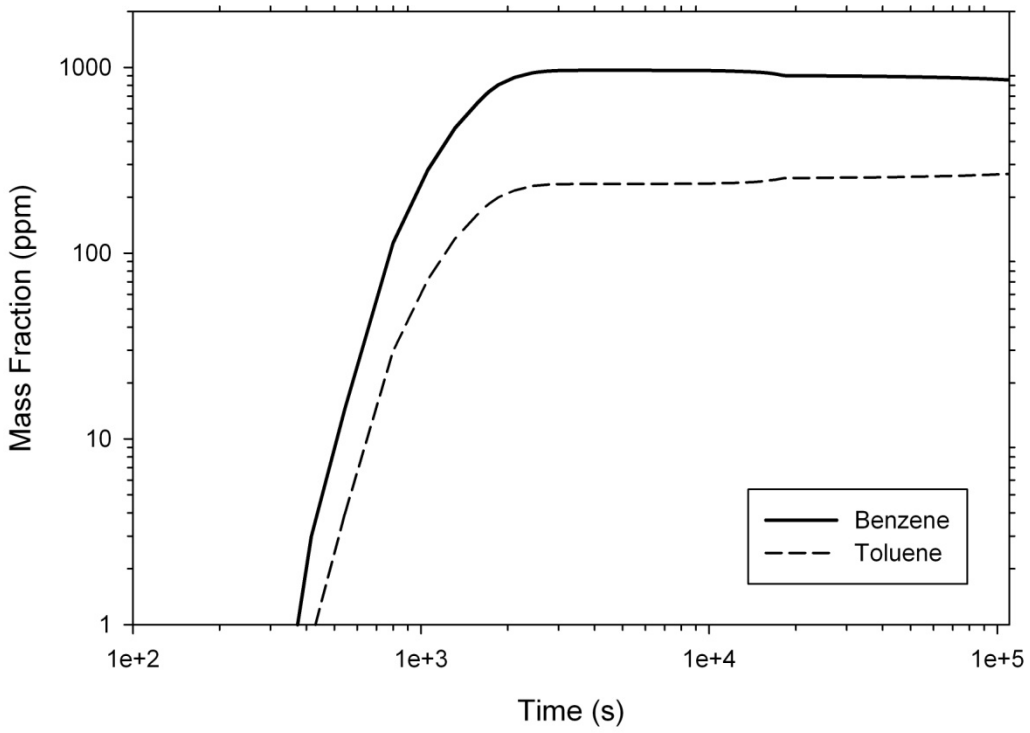

Figure B-3 – Re-created Figure 10.5.6 from the TMVOC Users Manual, Example Problem No. 5 to demonstrate model calibration.

Figure B-3 shows that the amount of benzene removed at the end of the waterflood is greater than the mass fraction of toluene removed. This occurs because the solubility of benzene is greater than toluene which allows the benzene to have more mobility.

Recreation of the Figures 10.5.5 and 10.5.6 from Example Problem 5 in the TMVOC users manual was successful in testing that the model was compiled correctly (as shown by the matching Figures B-2 and B-3).

Literature Cited

Pruess, K., & Battistelli, A. 2002. *TMVOC, A Numerical Simulator for Three-Phase Non-isothermal Flows of Multicomponent Hydrocarbon Mixtures in Saturated-Unsaturated Heterogeneous Media.* Lawrence Berkeley National Laboratory, Berkeley, CA.

Falta, R.W., Pruess, K., Javandel, I., & Witherspoon, P.A. 1992. *Numerical Modeling of Steam Injection for the Removal of Nonaqueous Phase Liquids From the Subsurface 2. Code Validation and Application.* Water Resources Research 28, 451-655.

Appendix C

TMVOC Model Input Property Definitions

C.1 Rock Properties

Density [kg/m^3] – The mass of a substance per unit volume of the substance.

Permeability [m^2] – Property of the soil or rock that dictates the ability of a fluid to move by advection. The permeability depends greatly on the pore size and pore connectivity.

Fraction of Organic Carbon – The fraction of organic carbon that is found naturally occurring in the subsurface. It is measured as mass of organic carbon per mass of soil or rock.

Formation Heat Conductivity [W/m·C] – Also known as the thermal conductivity of a material, it is quite variable for different rock types. It is highly dependent on saturation and temperature changes. The heat conductivity can be for liquid saturated or desaturated conditions. The reader is referred to Chapter 2.0 Literature Review for further details.

Rock Grain Specific Heat [J/kg·C] – Also known as the specific heat capacity, is the amount of energy that is required to increase the temperature of a material by 1 degree Celsius.

Porosity – The ratio of volume of the void space of a porous material to the total volume of the material. Changes in porosity occur when there is a change in temperature and pressure. It is defined by Reid et al, (1987) and TMVOC uses the following equation (Falta et al., 1992):

$$\emptyset = \emptyset_R[1 + \varepsilon_P(P - P_R) + \varepsilon_T(T - T_R)] \quad \text{(C.1)}$$

where $\emptyset_R$ is the reference porosity of the material, ε_p is the pore compressibility and ε_T is the expansivity and are both assumed to be constant. *P* and *T* represent the pressure and temperature being applied to the system with P_R and T_R being the reference pressure and temperature respectively.

Pore Compressibility [Pa^{-1}] – When there is change in pressure, compression of the pores in the rock matrix occurs. The reader is referred to Chapter 2.0 Literature Review for further details. It is implemented into the model using the following (Pruess & Battistelli, 2002):

$$\varepsilon_P = \left(\frac{1}{\emptyset}\right)\left(\frac{\partial \emptyset}{\partial P}\right)_T \quad \text{(C.2)}$$

where ε_p is the pore compressibility, $\emptyset$ is the porosity, and $\partial\emptyset/\partial P$ is the change in porosity with respect to pressure at a constant time, *T*.

Pore Expansivity [$°C^{-1}$] – The change in porosity when expansion occurs in response to a change in temperature with a constant pressure. TMVOC applies the following equation (Pruess & Battistelli, 2002):

$$\varepsilon_T = \left(\frac{1}{\emptyset}\right)\left(\frac{\partial \emptyset}{\partial T}\right)_P \quad \text{(C.3)}$$

where ε_T is the pore expansivity, and $\partial\emptyset/\partial T$ is the change in porosity with respect to temperature at a constant pressure, *P*.

Tortuosity Factor – The actual travel distance through a porous medium divided by the straight-line travel distance. When the tortuosity factor for binary diffusion is set to 0, TMVOC calculates the gas phase tortuosity, τ_g, using the Millington and Quirk Model (1961) which uses the porosity, $\emptyset$, and the gas phase saturation, S_g as follows (Falta et al., 1992):

$$\tau_g = \emptyset^{1/3} {S_g}^{7/3} \tag{C.4}$$

Klinkenberg Parameter – The slip flow of a gas in a pore, which reduces the drag forces and in turn enhances the gas flow through the pores (Webb, 2001). It is important when the permeability of the media is less than 10^{-18} m^2 and at low differential pore pressures (Webb and Preuss, 2003). TMVOC calculates the absolute permeability of the gas phase according to (Pruess & Battistelli, 2002):

$$k = k_\infty \left(1 + \frac{b}{P}\right) \tag{C.5}$$

where k_∞ is the permeability at "infinite" pressure, b is the Klinkenberg parameter and P is the pressure. The Klinkenberg parameter can be estimated using the Jones and Owens (1980) equation for low permeability sands in the range of 10^{-14} to 10^{-19} m^2 (Webb & Pruess, 2003) as follows:

$$b = {k_o}^{-0.33} \tag{C.6}$$

where k_o is the intrinsic permeability in m^2.

C.2 Chemical Properties

Diffusion – Movement (non-advective) of a solute from a region of high concentration to a region of low concentration. The diffusive flux (one-dimensional) is represented by Fick's Law (Fetter, 2001):

$$F = -D\frac{dC}{dx} \tag{C.7}$$

where *F* is the mass flux of the solute, *D* is the diffusion coefficient of the solute, *C* is the solute concentration and *dC/dx* is the concentration gradient.

Literature Cited

Falta, R.W., Pruess, K., Javandel, I., & Witherspoon, P.A. 1992. *Numerical Modeling of Steam Injection for the Removal of Nonaqueous Phase Liquids From the Subsurface 1. Numerical Formulation.* Water Resources Research 28, 433-449.

Falta, R.W., Pruess, K., Javandel, I., & Witherspoon, P.A. 1992. *Numerical Modeling of Steam Injection for the Removal of Nonaqueous Phase Liquids From the Subsurface 2. Code Validation and Application.* Water Resources Research 28, 451-655.

Fetter, C.W. 2001. *Applied Hydrogeology: Fourth Edition*. Prentice Hall, New Jersey.

Pruess, K., & Battistelli, A. 2002. *TMVOC, A Numerical Simulator for Three-Phase Non-isothermal Flows of Multicomponent Hydrocarbon Mixtures in Saturated-Unsaturated Heterogeneous Media.* Lawrence Berkeley National Laboratory, Berkeley, CA.

Reid, R.C., Prausnitz, J.M., & Poling, B.E. 1987. *The Properties of Gases & Liquids Fourth Edition.* McGraw-Hill, United States.

Webb, S.W. 2001. *Modification of TOUGH2 to Include the Dusty Gas Model for Gas Diffusion.* Sandia National Laboratories, Livermore, California.

Webb, S.W., & Pruess, K. 2003. *The Use of Fick's Law for Modeling Trace Gas Diffusion in Porous Media.* Transport in Porous Media 51, 327-341.

Appendix D

Calculations

D.1 Fracture Aperture and Permeability

Hydraulic tests employing a straddle packer assembly were conducted in the three well holes in which the rock samples were taken, BR-1, BR-2 and BR-3. The hydraulic testing was completed by TerraTherm Inc. prior to the pilot test heating. From the hydraulic testing, TerraTherm Inc. calculated the hydraulic conductivity. The fracture aperture to be incorporated into the TMVOC simulation was calculated using the results of these hydraulic tests. The measured transmissivity (*TR*) of the tested interval length (*l*) is related to the bulk rock hydraulic conductivity (*K*) through (Fetter, 2001):

$$TR = Kl \tag{D.1}$$

If it is assumed that the rock matrix permeability is negligible compared to that of the fracture, then the measured transmissivity can be related to the fracture hydraulic aperture (*e*) through (de Marsily, 1986):

$$TR = \frac{\rho g}{12\mu}(e)^3 \tag{D.2}$$

where ρ is the water density, g is gravitational acceleration, μ is the viscosity of water and *e* is the fracture aperture. Rearranging this equation, the fracture aperture can be calculated as (with results displayed in Tables D-1 to D-3):

$$e = \sqrt[3]{\frac{12TR\mu}{\rho g}} \tag{D.3}$$

It is assumed here that the groundwater temperature is approximately 10 degrees Celsius and thus the density of water was 1 g/cm^3 and the viscosity was 0.01 g/s·cm (Fetter 2001).

The rock permeability can also be calculated using the packer testing results. The permeability is calculated as:

$$k = \frac{K\mu}{\rho g} \tag{D.4}$$

Table D-1- Hydraulic test and aperture calculation results for BR-1 (hydraulic conductivity calculated by TerraTherm Inc.; transmissivity and fracture aperture calculated by Ashley McKenzie).

Date	Packer Depth (ft)	Well Depth (ft)	Packer Interval b (ft)	Hydraulic Conductivity K (cm/s)	Transmissivity T (cm^2/s)	Fracture Aperture 2b (cm)	Average Aperture 2b (μm)	Permeability (m^2)
11/21/2008	11	21	10	3.15E-05	9.60E-03	1.05E-02	99	3.21E-14
				2.29E-05	6.97E-03	9.48E-03		2.33E-14
				2.41E-05	7.35E-03	9.65E-03		2.46E-14
11/21/2008	21	31	10	2.73E-04	8.33E-02	2.17E-02	198	2.79E-13
				1.96E-04	5.99E-02	1.94E-02		2.00E-13
				1.67E-04	5.09E-02	1.84E-02		1.70E-13
11/21/2008	31	41	10	1.12E-04	3.42E-02	1.61E-02	160	1.14E-13
				9.90E-05	3.02E-02	1.55E-02		1.01E-13
				1.16E-04	3.55E-02	1.63E-02		1.19E-13
11/21/2008	41	51	10	9.49E-05	2.89E-02	1.52E-02	141	9.68E-14
				7.92E-05	2.41E-02	1.43E-02		8.07E-14
				5.66E-05	1.72E-02	1.28E-02		5.77E-14

Table D-2- Packer test and aperture calculation results for BR-2 (hydraulic conductivity calculated by TerraTherm Inc.; transmissivity and fracture aperture calculated by Ashley McKenzie).

Date	Packer Depth (ft)	Well Depth (ft)	Packer Interval b (ft)	Hydraulic Conductivity K (cm/s)	Transmissivity T (cm^2/s)	Fracture Aperture 2b (cm)	Average Aperture 2b (μm)	Permeability (m^2)
11/20/2008	16	26	10	1.97E-04	5.99E-02	1.94E-02	194	2.01E-13
11/20/2008	26	36	10	0.00E+00	-	-	145	-
				0.00E+00	-	-		-
				5.65E-05	1.72E-02	1.28E-02		5.76E-14
				1.14E-04	3.47E-02	1.62E-02		1.16E-13
11/20/2008	36	46	10	0.00E+00	-	-	117	-
				1.55E-05	4.74E-03	8.34E-03		1.58E-14
				9.24E-05	2.82E-02	1.51E-02		9.42E-14
11/20/2008	46	56	10	8.82E-06	2.69E-03	6.90E-03	85	9.00E-15
				2.01E-05	6.12E-03	9.08E-03		2.05E-14
				2.21E-05	6.73E-03	9.38E-03		2.25E-14

Table D-3 - Packer test and aperture calculation results for BR-3 (hydraulic conductivity calculated by TerraTherm Inc.; transmissivity and fracture aperture calculated by Ashley McKenzie).

Date	Packer Depth (ft)	Well Depth (ft)	Packer Interval b (ft)	Hydraulic Conductivity K (cm/s)	Transmissivity T (cm^2/s)	Fracture Aperture 2b (cm)	Average Aperture 2b (μm)	Permeability (m^2)
11/19/2008	11	21	10	4.72E-05	1.44E-02	1.21E-02	116	4.82E-14
				3.05E-05	9.29E-03	1.04E-02		3.11E-14
				5.03E-05	1.53E-02	1.23E-02		5.13E-14
11/19/2008	21	31	10	0.00E+00	-	-	83	-
				0.00E+00	-	-		-
				5.16E-06	1.57E-03	5.77E-03		5.26E-15
				3.75E-06	1.14E-03	5.19E-03		3.82E-15
				7.05E-05	2.15E-02	1.38E-02		7.19E-14
11/19/2008	31	41	10	2.99E-04	9.12E-02	2.23E-02	191	3.05E-13
				1.65E-04	5.03E-02	1.83E-02		1.68E-13
				1.22E-04	3.71E-02	1.66E-02		1.24E-13
11/19/2008	41	51	10	6.19E-05	1.89E-02	1.32E-02	102	6.31E-14
				2.58E-05	7.87E-03	9.88E-03		2.63E-14
				1.63E-05	4.97E-03	8.47E-03		1.66E-14
				1.99E-05	6.06E-03	9.05E-03		2.03E-14

D.2 Klinkenberg Coefficient

The Klinkenberg coefficient was calculated using Equation D.4 as given by Jones and Owens (1980) for low permeability sands having a permeability value between 10^{-19} and 10^{-14} m^2 (Webb and Pruess, 2003). The average bulk rock permeability (k_o) at the Naval Air Warfare Centre test site in Trenton, New Jersey is 9.79E-18 m^2 (Rodriguez et al., 2012) and b_{air} is the Klinkenberg parameter. The resulting Klinkenberg coefficient used for the 2D numerical model simulations was 2.4 x 10^{-6} Pa^{-1}.

$$Klinkenberg\ Coefficient = \frac{1}{b_{air}} = {k_o}^{-0.33} \tag{D.4}$$

D.3 Rock Pore Compressibility

The pilot test occurred primarily in a highly weathered grey mudstone which is classified as a sedimentary rock. The compressibility of rock can be highly variable and was not measured during the NAWC pilot test. The pore compressibility of the mudstone was calculated using the information from Zimmerman (1991) on pages 29-30 (compressibility values for several sandstone reservoirs). The average pore compressibility was calculated from twenty-four reservoir sandstones. The rock pore compressibility, ε_p, is calculated using Equation D.5.

$$\varepsilon_p = \frac{\varepsilon_b - C_r}{\emptyset} \tag{D.5}$$

where ε_b is the bulk compressibility, C_r is the addition factor given by Fatt (1958a) as 1.8x10^{-7} psi^{-1} and ø is the porosity of the sandstone. The average rock pore compressibility was calculated to be 3x10^{-9} Pa^{-1}.

D.4 Fracture Zone Cell Permeability

The permeability of the fracture zone cell can be calculated using the permeability found from the packer tests and analytical tests using:

$$k_b = \frac{k_m(\Delta z_m) + k_f e}{(\Delta z_m + e)} \quad \text{(D.6)}$$

where k_b is the bulk permeability from the packer testing which is equal to 8.4×10^{-14} m^2, k_m is the matrix permeability from analytical testing set to 9.79×10^{-18} m^2 and Δz_m is the packer spacing equal to 3.048 m. The permeability in the field of the fracture (k_f) is calculated using Equation D.7 below and substituted in Equation D.6.

$$k_f = \frac{e^2}{12} \quad \text{(D.7)}$$

The fracture zone permeability (k_{fz}) used for the numerical model simulations is calculated using Equation D.8 as developed by Baston et al. (2010).

$$k_{fz} = \frac{k_f \cdot e + k_m(\Delta z_{fz} - e)}{\Delta z_{fz}} \quad \text{(D.8)}$$

where Δz_{fz} is the cell thickness in the model for the fracture zone which was set to 1 cm. The resulting permeability values used in the numerical 2D model is 1×10^{-17} m^2 for used as the bulk rock matrix and 1×10^{-11} m^2 which is the fracture zone permeability for the three fractures.

D.5 Mole Fraction of TCE

To include TCE in the model, TMVOC requires it to be in the form of a mole fraction. The initial concentration of TCE estimated from the pre-heating rock samples was used to calculate the values used in the model. It was assumed that only the sorbed and aqueous phase is present and the following equation was used to calculate the aqueous TCE concentration (Kueper and Davies, 2009):

$$C_T = \frac{C_i}{\rho_b}(K_d\rho_b + \emptyset_w + H'^{\emptyset_a}) \tag{D.9}$$

where C_T is the soil concentration, the dry soil bulk density of 2520 kg/m^3, K_d is the soil-water partition coefficient and is equal to $k_{oc} \cdot f_{oc}$. The value used for the organic carbon partition coefficient, k_{oc}, is 126 mg/L which is the standard value for TCE, and f_{oc}, the fraction of organic carbon measured by the laboratory was found to be 0.00785. The water-filled porosity, $\emptyset_w$, is equal to the porosity as the soil is assumed to be saturated and is 0.033. Since there is no air present in the system, the air-filled porosity, $\emptyset_a$, is set to zero. Rearranging Equation D.9 to solve for C_i, the effective solubility in mg/L is as follows:

$$C_i = \frac{C_T\rho_b}{K_d\rho_b + \emptyset_w} \tag{D.10}$$

The effective solubility can be converted into units of mol/L by dividing C_i by the molecular weight of trichloroethylene (131.39 g/mol). The mole fraction is calculated using Equation D.11 below and a molecular weight of water (C_w) of 55.46 mol/L.

$$[TCE] = \frac{C_i}{C_w + C_i} \quad \text{(D.11)}$$

Literature Cited

Baston, D.P., Falta, R.W., & Kueper, B.H. 2010. *Numerical Modeling of Thermal Conductive Heating in Fractured Bedrock.* Ground Water 48: 836-843.

de Marsily, G. 1986. *Quantitative hydrogeology. Groundwater hydrology for engineers.* Academic, New York.

Fatt, I. 1958a. *Compressibility of sandstones at low to moderate pressures.* Bulletin of the AAPG 42, 1924-1957.

Fetter, C.W. 2001. *Applied Hydrogeology: Fourth Edition*. Prentice Hall, New Jersey.

Kueper, B.H. and Davies, K.L., 2009. *Assessment and delineation of DNAPL source zones at hazardous waste sites.* United States Environmental Protection Agency, Publication EPA/600/R-09/119.

Rodriguez, D.J., and Kueper, B.H. 2012. *Assessment of Thermal Conductive Heating for the Remediation of DNAPL Contaminated Fractured Bedrock.* (In Progress).

Webb, S.W., & Pruess, K. 2003. *The Use of Fick's Law for Modeling Trace Gas Diffusion in Porous Media.* Transport in Porous Media 51, 327-341.

Zimmerman, R.W. 1991. *Compressibility of sandstones*, Developments in Petroleum Science 29, Elsevier, New York, NY, USA.

Appendix E

Fixed versus No-Flow Bottom Boundary Condition

The bottom boundary in numerical model simulations was extended 10.5 m below the bottom of the treatment zone in order to reduce the influence of the bottom boundary condition on the model results. There were two different bottom boundary conditions examined when setting up the baseline model simulations, a fixed boundary and a no-flow boundary.

A fixed boundary is set with a constant pressure and temperature during the model simulations which forces those boundary conditions to always be met at that boundary. A no-flow boundary is essentially a confining layer that does not allow any fluid or temperature cross the boundary. The baseline model (with a matrix permeability of $1x10^{-15}$ m^2) was run with both bottom boundary conditions and compared to examine the effects the different boundaries created on the TCE removal from the rock matrix.

The two model simulations were compared at the observation location for Figures E-1 to E-3 to examine the difference in temperature, pressure, gas saturation and TCE extraction at four different time steps:

- 30 days which is in the heating phase;
- 40 days which is when the maximum average temperature is reached; and,
- 50 and 80 days during the period of constant heating.

Figure E-1 demonstrates that there is no significant difference in the temperature profiles at the observation location between the two boundary conditions.

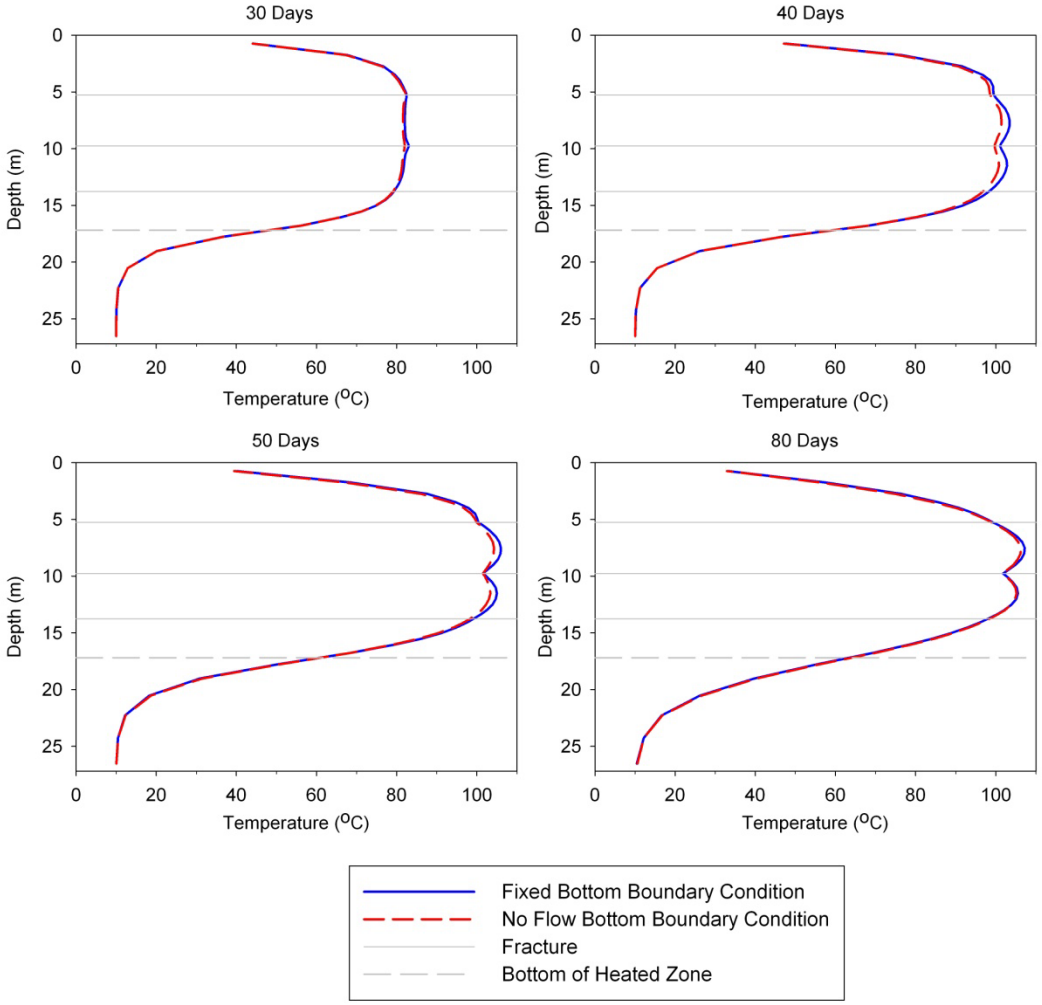

Figure E-1 – Model-predicted temperature profile in the rock matrix at the observation location over time.

A similarity in pressure profiles was also seen at the observation location between the two boundary conditions (Figure E-2).

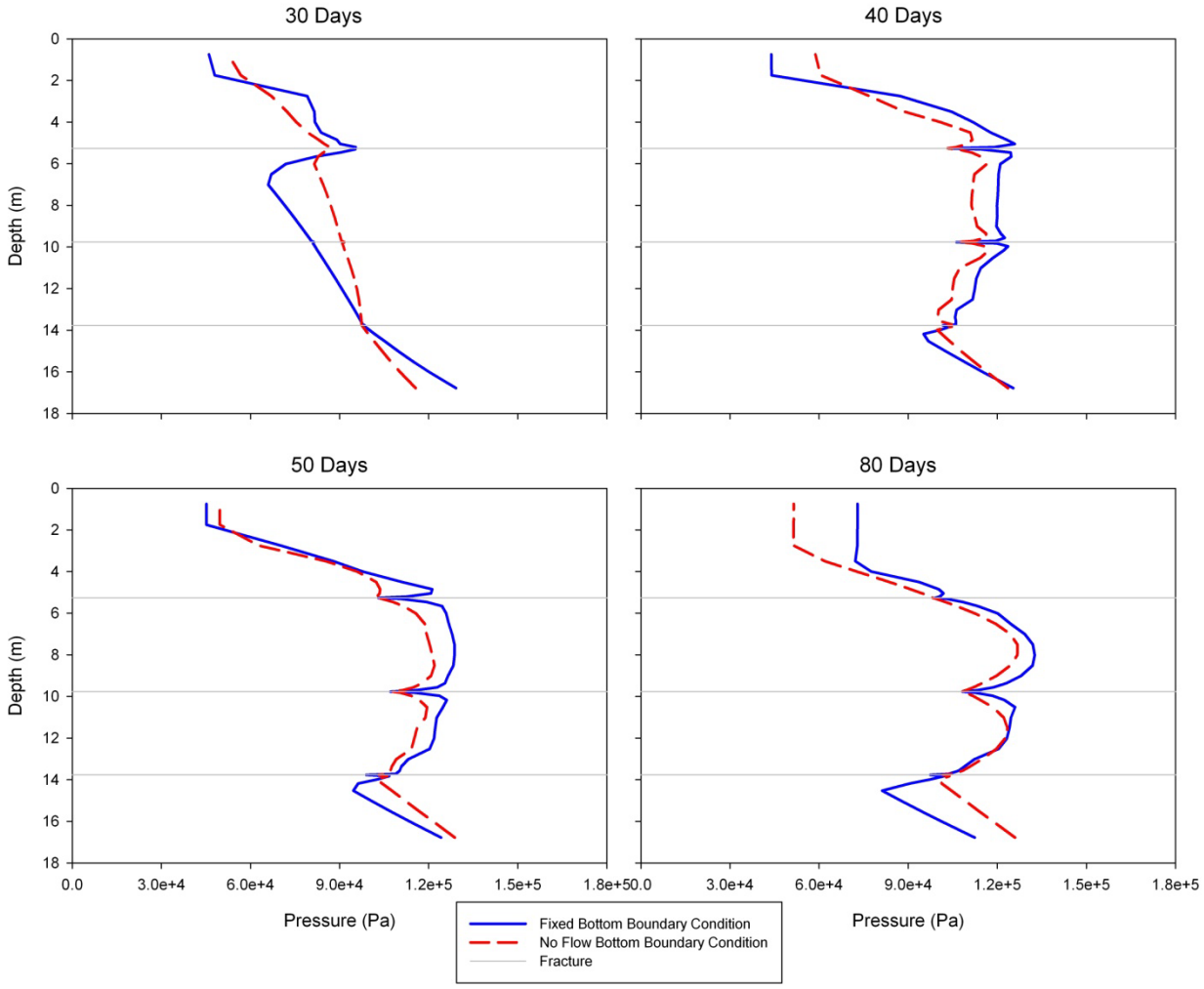

Figure E-2 – Model-predicted pressure profile in the rock matrix at the observation location over time.

The primary difference was displayed through the gas saturation profiles. Figure E-3 displays the difference between the gas saturation profiles in the fixed bottom boundary and no-flow bottom boundary simulations at the observation location. The figure displays that the boundaries have a significant effect on the gas saturation in the rock matrix during heating.

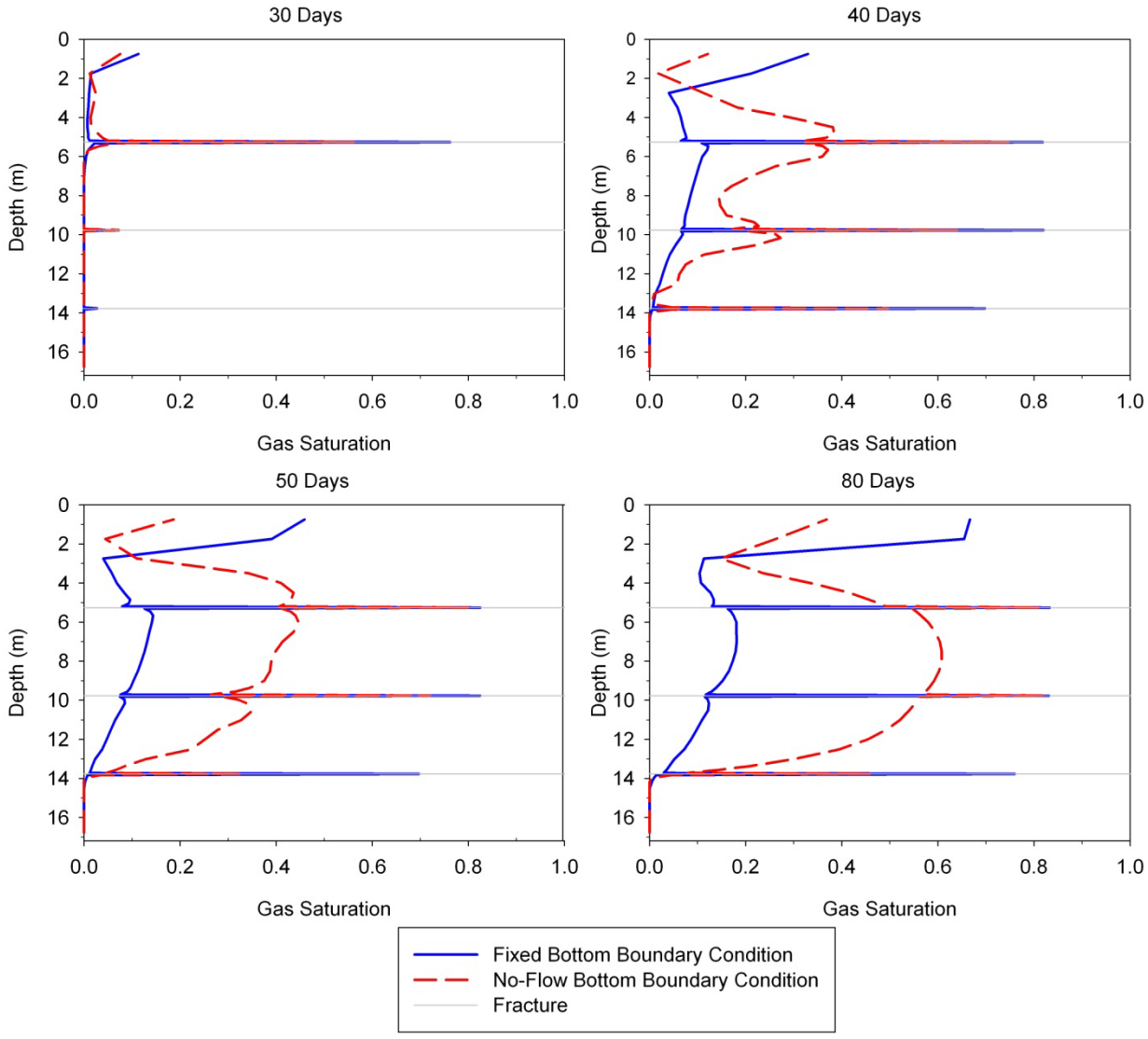

Figure E-3 – Model-predicted gas saturation profile in the rock matrix at the observation location over time.

The profiles show that at 30 days there is little difference between the gas saturation profiles with the different boundary conditions. When the maximum temperature is reached at 40 days, the saturation profile becomes quite different between the two boundaries. The fixed bottom boundary condition shows a less gas saturation in the rock matrix than the no-flow bottom boundary condition for 40, 50 and 80

days. This is because the fixed boundary condition allows the model to “fill” back up with water therefore reducing the gas phase (this is due to the constant pressure being fixed at the bottom boundary).

When the TCE in the rock matrix is converted from the liquid phase to the gas phase it is easier to extract. Figure E-4 displays the TCE profile in the rock matrix over time. The TCE concentration for the no-flow bottom boundary is always less than that observed in the fixed bottom boundary simulation. The no-flow bottom boundary resulted in 67% TCE removal from the rock matrix compared to the fixed bottom boundary which had 44% TCE removal.

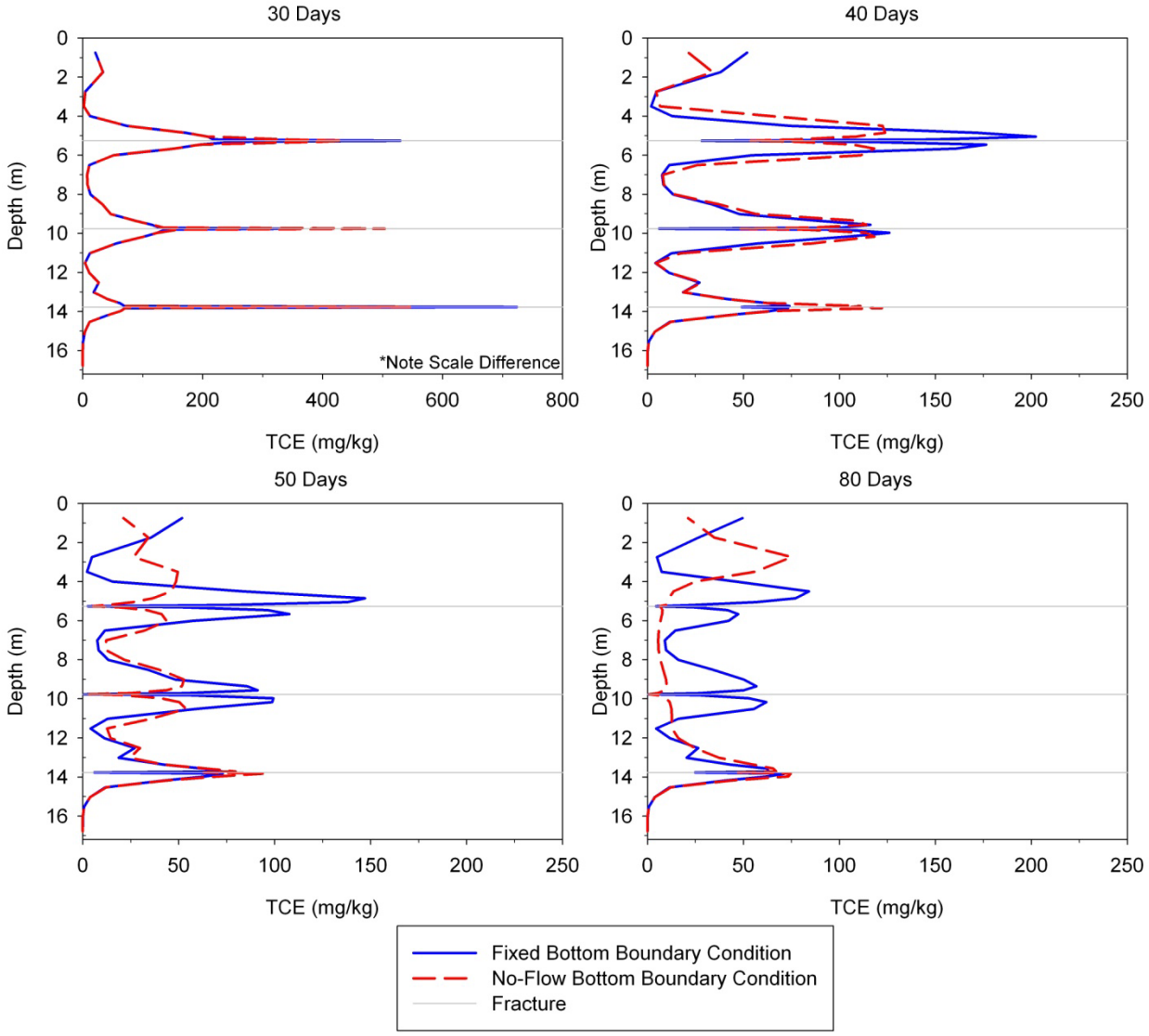

Figure E-4 – Model-predicted TCE profile in the rock matrix at the observation location over time.

Although both boundary conditions are located 10.5 m away from the heating zone there is a significant effect on the amount of gas that is created in the rock matrix during heating. This difference allows for more TCE to be removed from the rock matrix in the no-flow bottom boundary than the fixed bottom boundary. The average percentage of TCE removed from the rock matrix during the NAWC pilot test after 100 days of heating was 63.5%. The rock matrix at the NAWC site becomes less fractured with

depth therefore it could be hypothesized that the lower permeability with depth acts to restrict the upward flow of water back into the heating zone. The no-flow bottom boundary condition acts in a similar way as a lower permeability zone which resulted in 67% removal from the rock matrix. These results concluded that a no-flow bottom boundary is more appropriate to use than the fixed bottom boundary condition and was therefore applied for all simulations.